"Defining the synaptic mechanisms that tune CA3-CA1 reactivation during sharp-wave ripples"

Paola Malerba[1], Matt W. Jones[2], Maxim A. Bazhenov[1]

[1] University of California San Diego, Department of Medicine, La Jolla 92093, USA

[2] University of Bristol, School of Physiology, Pharmacology & Neuroscience, Bristol BS8 1TD, UK

Short Title: Mechanisms of ripple replay

Corresponding Author: Maxim Bazhenov, University of California San Diego Department of Medicine

9500 Gilman Drive # 7381, La Jolla, CA 92037

Email mbazhenov@ucsd.edu

Conflict of Interest: The authors declare no competing financial interests.

Abstract

During non-REM sleep, memory consolidation is driven by a dialogue between cortex and hippocampus. The reactivation of specific neural activity sequences – replay – is believed to represent a neuronal substrate of consolidation. In the hippocampus, replay occurs during sharp-wave ripples (SWRs), short bouts of excitatory activity in area CA3 which induce high frequency oscillations in the inhibitory population of area CA1. Despite growing evidence for the functional importance of replay, its neural mechanisms remain poorly understood. Here, we develop a novel theoretical model of hippocampal spike sequence replay during SWRs. In our model, noise-induced activation of CA3 pyramidal cells triggered an excitatory cascade, which induced local ripple events in CA1. Ripples occurred stochastically in the model, with Schaffer Collaterals driving coordination, so that localized sharp waves in CA3 produced consistently localized CA1 ripples. In agreement with experimental data, the majority of pyramidal cells in the model showed low reactivation probability across SWRs, defined by the overall network connectivity. We found, however, that a small portion of pyramidal cells which had high reactivation probability across multiple SWRs owed their reactivation properties to the fine variations within network connectivity, and hence the detailed spiking dynamic within SWRs. In particular, the excitatory inputs along synaptic pathway(s) to cells and cell pairs controlled emergent single cell and cell pair reactivation. Furthermore, we found that inhibitory synaptic inputs and intrinsic cell excitability only had an influential role on the activation of CA3 pyramidal cells, but not CA1 pyramidal cells, during SWRs. Our study predicts that hippocampal replay results from a network-wide coordination of activation probability across SWRs for cells and cell pairs, which is further refined by specific synaptic strengths. This suggests a possible competition among cell assemblies for activation during SWRs, where synaptic strengths mediate the chance of dominance of a given memory over others during spontaneous SWRs.

Author Summary

During sleep, rhythmic activities in different brain regions are coordinated across multiple timescales and brain regions. The coordination of these events is important for consolidation of recently acquired memories. Sharp-wave ripples (SWRs) are one of such major sleep rhythms, seen in the hippocampal region, during which cells previously active during an awake task reactivate, in preserved order, during sleep ('replay'). Replay is thought to contribute to consolidation by enabling re-elaboration of events of the day during sleep. However, the manner in which specific spiking patterns are selected for replay remains unknown. In this study, we apply computational models to reveal mechanisms behind the generation of SWRs and to explain the factors controlling which cell sequences reactivate during SWRs. We find that different hippocampal regions have different factors that promote replay. Our study predicts that when learning changes the strength of synaptic connections during wake, it would enhance the probability of reactivation of experience-specific groups of neurons during sleep.

Introduction

Memories acquired during wakefulness continue to evolve during subsequent sleep. Sleep seems an optimal brain state for this memory consolidation: the brain is dissociated from external inputs and internal processing can be supported by sleep stage-dependent patterns of network activity, driven largely by periodic shifts in neuromodulatory tone (1, 2). During non-REM sleep, hippocampal networks show sharp-wave ripples (SWRs): short bouts of synchronized population activity (50-100ms) initiated in the CA3 area of the hippocampus with strong excitatory firing that reaches area CA1, driving fast spiking interneurons to rhythmically organize a small fraction of local pyramidal cells spiking (3-5). In CA1, local field potential (LFP) high frequency oscillations (above 150Hz in the rat, about 100Hz in humans) occur in the pyramidal layer (the ripple), while in *stratum radiatum* a strong deflection marks the effects of Schafferal Collateral input to the pyramidal cells (the sharp wave). Hippocampal SWRs can be locked to cortical slow oscillations (SO) and troughs of

63 thalamocortical spindles, in a coordination of activity across brain regions and time scales (6, 7),
64 which is thought to orchestrate a hippocampal-neocortical dialogue mediating memory
65 consolidation.

66 The number of SWR correlates with memory performance after sleep (8, 9), suppressing SWR
67 compromises memory consolidation (10, 11) and increased SO power and coordination of SO and
68 other sleep rhythms augments memory (12). Reactivation of specific neural activity patterns – replay
69 – during slow wave sleep has been observed in both hippocampus and neocortex (13-18), and
70 coincides with SWR (19, 20). This led to the hypothesis that coordinated sequence reactivation
71 during precisely timed oscillations can recruit synaptic plasticity, leading to memory consolidation
72 across brain structures (21). Within this hypothesis, understanding how replay happens in
73 hippocampal SWR is crucial to explain sleep dependent memory consolidation.

74 CA1 pyramidal cells are not homogeneous with respect to activity during ripples, and can be sub-
75 classified into those that spike during ripples and those that do not; these properties seem to remain
76 stable across sleep epochs (3, 22, 23). Furthermore, recent experimental data show that comparing
77 sleep reactivation before and after a learning experience allows identification of cells for which
78 reactivation during SWR remains unchanged by learning and (separate) cells which show increased
79 ripple spiking during learning and subsequent sleep (24). Together, these data support a framework
80 in which hippocampal reactivation incorporates a relatively large set of cells which activate during
81 ripples regardless of recent learning, and a smaller group of cells which are involved in reactivation
82 because of experience-dependent changes in their connectivity. In the simplest scenario, the precise
83 content of hippocampal sequence reactivation is shaped by the hippocampal synaptic circuitry, with
84 afferents (e.g. entorhinal or thalamic) potentially eliciting a generic reactivation prompt.

85 In this work, we address a question on the mechanism of hippocampal reactivation using a
86 biophysical network model of CA3-CA1 SWR activity, where spontaneous, localized and stochastic
87 excitatory events in the highly recurrent CA3 network drive transient oscillations in CA1 inhibitory

interneurons, which in turn only leave small windows of opportunity for CA1 pyramidal cells to spike. Our model reveals a mechanism of emergent, spontaneous activation of pyramidal cells across SWRs, and predicts how learning can affect the specific reactivation of the hippocampal neurons which is seen during sleep, while global network behavior is supported by the network architecture.

Results

Computational model of spontaneous, localized SPW-R activity

In our previous work (25), we introduced a model of CA1 ripples in which oscillations in the LFP were due to a transient in the system dynamics (as opposed to a stable oscillatory state), imposed by fast firing of the basket cells initially synchronized by common current input (representing CA3 excitation), which lost coordination in time due to the cell population heterogeneity. Here we build on that work to introduce a model of CA3-CA1 SWRs in which CA3 activity emerges spontaneously and triggers stochastic activation of the SWR events in CA3 and CA1, with the termination of ripples driven by the same de-coordination mechanism that we previously described in CA1 (25). In the new model, different subsets of cells were involved across different SWR events as observed experimentally (26).

This model of CA3-CA1 SWR activity is based on synaptically coupled populations of pyramidal cells and basket cells (Figure 1A). The model included highly recurrent strong excitatory AMPA receptor-mediated connections between CA3 pyramidal cells, and weak and sparse recurrent excitatory connections within CA1 pyramidal cells (27). CA3 pyramidal cells projected excitatory connections to CA1 cells, representing the Schaffer Collaterals. The CA3 network and its projections to CA1 had stochastic densities and strengths within a radius of about a third of the target network (28) (Figure 1B shows a matrix the presence of synaptic connections), which is consistent with analysis of CA3 pyramidal cells arborization (28). Importantly, each neuron received an independent noise current which drove occasional irregular spiking, and a baseline constant drive which was selected from a

distribution. Details of the computational model rationale and equations are reported in Materials and Methods.

Figure 1. Computational Model of emergent, localized SPW-R activity

A. *Schematic representation of the model, showing the two main regions (CA3 and CA1) and the cell types considered (pyramidal cells and basket cells). Note that CA3 projects to CA1, but not vice-versa.* ***B.*** *Matrix representation of presence of synaptic connections in the model. Synaptic weights are not shown, hence darker tone is only indicative of local higher density of connections. Note that CA3 pyramidal cells connect to all cell types in the network.* ***C.*** *Example of SPW-R activity in the network. Top 2 plots: raster plots of cell spikes (CA3 above, CA1 below). Dots mark spikes in time of pyramidal cells (black) and interneurons (red). In CA3 sharp waves happen at different locations and show different propagation patterns in time. CA1 spiking is organized by the sharp waves in CA3, and ripples are visible as small sharp stripes of dense spiking in CA1 pyramidal cells. Bottom two plots: Local Field Potential (LFP) of the model, computed as the average of the total incoming synaptic currents across a group of pyramidal cells. Note that in CA3 we show the wide-band signal, to highlight the sharp transition occurring in the synaptic currents when a sharp wave is present in the CA3 network. At corresponding times (and locations) in the LFP of CA1 (filtered in ripple range) one can see the high frequency activity captured by the LFP signal.* ***D.*** *Zoomed-in raster plot of spiking activity in CA3 and CA1, the time window is indicated by the arrow in C. SWR activity is localized within the two regions. For each sharp wave (SPW) and each ripple (RPL) a center (or location) can be defined as the medium index among the pyramidal cells which spike during the event. The LFPs shown on the right refer to groups of cells slightly apart in the network, shown as colored rectangles in the rastergram. Note that some SWR can be seen in the LFP traces at both locations (near 11s) while others are only visible in one of the traces (about 400ms later).*

As shown in Figure 1C, the network spontaneously organized into strong bouts of CA3 pyramidal cell spiking, which drove spiking in CA1. In CA1, interneurons organized their firing in high frequency oscillations, and a few pyramidal cells spiked within windows of opportunity left at the troughs of the lateral synaptic inhibition oscillations, thus forming a SWR event. SWRs occurred in temporal clusters punctuated by long pauses. A representation of the local field potentials (LFPs) obtained by averaging the synaptic currents impinging on subsets of pyramidal cells showed that SWR events in CA3 and CA1 were localized, and the location of the SWRs within the network changed in time. This is consistent with experimental findings that show that ripple events can be localized in space (26, 29) and that CA3 pyramidal cells are known to be very active during SWR, but do not spike phase-locked to CA1 ripples (30, 31).

Figure 1D shows a zoomed-in version of the SWR spiking activity and LFPs in sub-regions of CA3 and CA1 which were connected by Schaffer Collaterals. Although sharp waves are typically experimentally measured in CA1 *stratum radiatum*, in the following we refer to sharp waves as the

bouts of excitatory activity in CA3 which lead to ripples in CA1. The general activity of the model was consistent with known properties of SWRs: ripple frequency was 174±21.3 Hz, ripple durations were 54±27 ms, sharp wave durations were 126±23ms and the inter-event pauses (time durations between two successive sharp waves in CA3 or ripples in CA1) showed distributions approximately exponential, which fitted to exponential functions with rates 1.08 Hz for sharp waves in CA3 and 1.2Hz for ripples in CA1 (3). Within this model, we studied the spontaneous activation of CA3 and CA1 pyramidal cells across multiple ripples, in relation to their synaptic properties.

Non-uniform cell activation probability shapes distribution of ripple activation scores in CA3 and CA1

Sequential cell reactivation has primarily been demonstrated in CA1 pyramidal cells during SWRs, but fewer data are available on CA3 pyramidal cell replay (32). In our model, we first characterized sequence replay by studying the activation of each single cell across many SWRs. For this, we derive a 'ripple activation score' (R-activation score), given by the percent of SWRs in which a given cell spiked at least once, in the course of a 100 s simulation (schematized in Figure 2A; e.g., a R-activation score of 100% would mean that the cell spiked in every SWR event). Generating R-activation scores across many simulations (Figure 2B) revealed that, on average, cells in CA3 activated across more ripples than cells in CA1. This was likely driven by the lower percentage of CA1 pyramidal cells involved in any given ripple compared to the population of CA3 pyramidal cells inducing a sharp wave (which is consistent with experimental data (22, 30, 33)). The distribution of R-activation scores in both regions showed a large positive tale, and in CA1 a fast decay. This is also consistent with data suggesting that firing rates during ripples are log-normally distributed (3, 5, 34, 35). One model of CA3 emergent sharp wave activity suggests that this could be related to the distribution of synaptic weights used to populate the network connectivity matrices (36).

Figure 2. R-activation in CA3 and CA1 is stationary for low score cells and dynamic for high score cells

A. *Drawing shows the definition of R-activation score for a pyramidal cell. The total number of SWR in which a cell spikes during a 100 second simulation is found, and compared to the total number of SWR in the simulation. This fraction is expressed as a percent as the R-activation score of the cell.* ***B.*** *Distribution of R-activation scores of CA3 and CA1 pyramidal cells computed across many simulations and reported as average count in any given single trial. CA1 pyramidal cells show a peak for 0% R-activation, and the mean R-activation scores for CA3 pyramidal cells is higher than CA1 pyramidal cells.* ***C.*** *Curves (one per simulation) mark the probability distribution of pyramidal cells in CA3 to be spiking in any given SWR. Cells were sorted by increasing probabilities. The average probability curve (across all curves for each sorted cell index) is marked by a black solid line, while dotted black lines represent the standard deviation around the mean.* ***D.*** *Same as panel C for CA1 pyramidal cells.* ***E.*** *Distributions of R-activation scores in CA3 pyramidal cells in a stationary sorting algorithm (thick line) and in the model (dotted line). Note that the stationary process and the model share the low-reactivation peak probability, but have different trends for high-reactivations: the stationary choice peaks at 60% and quickly decays to zero for higher scores, while the model does not show peaks at high R-activation values (only the low R-activation peak is present) and has a larger amount of very high R-activations.* ***F.*** *Same as panel E for CA1 pyramidal cells: again stationary choice and computational model share the low R-activation peak and the model does not show a peak for intermediate levels of R-activation.*

The distribution of R-activation scores (Figure 2B) tells how many cells are likely to activate in a given fraction of all SWR, while the probability of spiking (Figure 2C,D) tells if a given cell is likely to activate in many or few SWRs (e.g., p=1 would mean that a cell spike in every SWR event). For each model simulation, we reported the probability of spiking in a SWR for all cells in CA3 and CA1 (in Figure 2 C-D). Since in every simulation new connectivity and heterogeneity profiles were generated (see Materials and Methods), we sorted the cells according to their spiking probability within SWRs, from lowest to highest. Then, it was possible to find an average distribution of such probabilities, and compare between CA3 and CA1 networks. In both cases, the variance around the mean increased for cells with higher SWR activation probabilities. The larger variations for high-probability cells (right side of the plots in Figure 2 C,D) suggested that all the cells fell in one of two categories: those which fired in very few ripples (the majority) and those which fired in a large fraction of ripples (above 0.6 probability).

Across many simulations, the rules which shaped network connectivity were fixed, but the actual specific network connections changed as they were generated probabilistically. This led to measurable variations in the properties of SWR activity, such as the total count of SWRs within

simulation time, and the size of ripples and sharp waves (as fraction of CA3 and CA1 pyramidal cells spiking during the event). In the following, we analyze the role of the stationary model properties: the ones that depend on the average model characteristics and do not change much across simulations (such properties included the distribution of ripple frequencies, of inter-event times, and the range of reactivation scores found across the population of pyramidal cells). We analyze separately the dynamic (or network-activity dependent) properties: those which are dependent on the specific model instantiation in a given simulation (such properties included a specific cell's spiking probability). To distinguish between the contributions of the stationary and network-activity dependent properties in shaping R-activation scores across simulations, we compared the distribution of R-activations that was found across simulations with a theoretical sampling model. This model was based on the average probability of spiking in CA3 and CA1 pyramidal cells (black lines in Figure 2 C-D). Thus, we sampled cells according to those probabilities, and we repeated the sampling 10,000 times and considered each sampling event a ripple in which the sampled cells had spiked. This sampling approach assumed that spiking in each SWR was memoryless and that the probability for a given cell to be spiking in any ripple was stationary (i.e. not changing in time within a simulation), so it was an extreme simplification of a complete computational model simulation. If the spiking of each cell across many SWRs in the complete model was independent of spiking history and activation of other cells, and only dependent on the average probability found in simulations, we should obtain in the simple theoretical model a sampling distribution of R-activation scores very similar (if not identical) to the ones in Figure 2B.

In Figure 2E-F we compared the stationary (sampling) distributions from the theoretical sampling model to those resulting from simulations: in both CA3 and CA1 we found that stationary R-activation (from the theoretical sampling model) showed a larger fraction of cells in the network having median R-activation scores (about 60% in CA3 and 40% in CA1) compared to the computational model, and very few cells showing very high R-activation scores (above 70% in CA3 and 60% in CA1). In other words, R-activation scores in the stationary case showed two peaks, one of

which at median activations, while in the simulations the second peak was removed, and a larger positive tale was found instead. We concluded that specific spiking dynamics of simulations (influenced by history dependence, slow variables and specific instances of network connectivity and excitability) promoted the long tales composed by cells with very high R-activation scores.

This analysis suggests that ripple activation in CA3 and CA1 was built on average on the stationary properties of the network architecture and overall network state, except for few highly-activating cells, whose properties were dependent on specific instantiation of the network architecture (such as, e.g., convergence of few strong excitatory connections to a given cell). Thus, the model predicts the co-existence of a relatively rigid structure in the CA3-CA1 network which enables the emergence and general properties of SWRs, with a specific network spiking activity in a subset of highly active neurons inducing replay during SWRs.

The influence of input on pyramidal cell R-activation

The network connectivity was set randomly for each simulation, and therefore specific synaptic paths connecting cells changed from one simulation to another, influencing how the ongoing spiking activity in the whole network could contribute to the R-activation score of a given cell. Since the SWRs in the model were induced by the spontaneously emergent excitatory activity in CA3, which controlled the spike timing of CA3 pyramidal cells and competed with CA1 local inhibitory ripple activity to drive the spikes of few CA1 pyramidal cells, we next studied the R-activation of pyramidal cells in relation to their incoming inputs. We considered synaptic excitatory and synaptic inhibitory inputs, together with intrinsic cell excitability.

We defined the excitatory and inhibitory synaptic input (S^{AMPA} and S^{GABA}, respectively, represented in Figure 3A) for each CA3 pyramidal cell by summing the synaptic weights of all incoming connections. The intrinsic excitability for each CA3 pyramidal cell corresponded to the value of model parameter I_{DC}, which was assigned (and different) to every cell to introduce heterogeneity among their resting potentials (see Materials and Methods, Network model: rationale). For each input, we next analyzed

the distribution of the input strength across R-activation scores (Figure 3B). All inputs considered (synaptic excitatory, inhibitory and intrinsic excitability) were on average higher for cells with higher R-activation scores, implying that all the inputs could contribute to enhancing the R-activation probability of a CA3 pyramidal cell.

Figure 3. In CA3 and CA1, pyramidal cell R-activation scores increase with excitatory input

A. *Drawing of the synaptic inputs analyzed for CA3 pyramidal cells. S^{AMPA} is the sum of all incoming AMPA connections (in black) to a CA3 pyramidal cell (labeled A) from other CA3 pyramidal cells (in gray). S^{GABA} is the sum of all incoming GABA connections (in red) to a CA3 pyramidal cell (A) from CA3 interneurons (in red).* ***B.*** *R-activation of CA3 pyramidal cells is related to strength of synaptic inputs and intrinsic excitability. The bar plot shows on the x –coordinate the average R-activation score of CA3 pyramidal cells belonging to the same score group (±5%) and on the y-coordinate the level of each different input (S^{AMPA}, S^{GABA} or Intrinsic Excitability) for cells within that score group. Error bars mark the standard error of the mean. Before grouping cells by their R-activation scores, each input was z-scored to enable comparisons of their respective trends. Therefore, a negative y-coordinate does not reflect a negative input, but an input below the average across the whole network.* ***C.*** *Drawing of the synaptic inputs analyzed for CA1 pyramidal cells. S^{Sch} (from CA3 to CA1, in green) is the sum of incoming AMPA synaptic weights from CA3 cells onto CA1 pyramidal cells. S^{Pre} (in black) for a given CA1 pyramidal cell (labeled x) finds all cells in CA3 that projects to x and their AMPA input (S^{AMPA}, described in* ***A****). The average value of all these S^{AMPA} inputs is S^{Sch}, representing the how much excitatory drive the cells in CA3 which project to x in CA1 are receiving. S^{GABA} is the sum of all incoming GABA connections (in red) to a CA1 pyramidal cell (x) from CA1 interneurons (in red).* ***D.*** *R-activation of CA1 pyramidal cells is related to synaptic excitatory input. The bar plot shows on the x –coordinate the average R-activation score of CA1 pyramidal cells belonging to the same score group (±5%) and on the y-coordinate the level of each different input (S^{Pre}, S^{Sch} or Intrinsic Excitability) for cells within that score group. Inputs were z-scored before grouping the cells by score. Error bars mark the standard error of the mean.*

To study role of the potential interactions among inputs in influencing cell R-activation, statistical inference analysis was performed using multivariate linear regression (see Table 1). For CA3, it showed significant modulation of R-activation by the three inputs (synaptic excitatory, synaptic inhibitory and intrinsic excitability). It also emphasized that the influence of synaptic excitatory input was captured in the interaction with the synaptic inhibitory input and with intrinsic excitability. When considered separately, the different inputs had a similar impact on R-activation, and combining the three inputs increased their ability to represent the R-activation data.

Table 1. Extract of linear regression models for R-activation of CA3 pyramidal cells vs inputs (from Table S1)

# Inputs	Inputs in Best Model	Model Equation Type	Adj. R-sq
3	AMPA,GABA,DC	quadratic, with AMPA-GABA interaction	0.249
2	AMPA,DC	quadratic, with AMPA-DC interaction	0.238

1	AMPA	Linear	0.146
1	GABA	Quadratic	0.11
1	DC	quadratic	0.0907

For each possible combination of the inputs that were considered (parameters of the model for the statistical linear fit), we found multiple fits to R-activation of CA3 pyramidal cells. When only one input at a time was considered, we found linear models of linear terms and linear models of quadratic terms. When multiple inputs were considered, we found linear models for linear terms, interactions and quadratic terms. We here report the models accounting for the larger portion of the data for each number of inputs considered, and all the single inputs best performing models. The complete list of models found is reported in Table S1. The adjusted R^2 terms can be interpreted as a measure of how much of the variance in the data is captured by a given model. As can be seen from the adjusted R^2 values, there was a high noise component in the relationship between inputs and CA3 cells R-activation. However, all models listed showed significant contributions of the inputs considered (by p-value<0.05 criterion).

For CA1 pyramidal cells, we isolated the role of the Schaffer Collateral projections by considering only the total strength of direct synaptic connections coming to a CA1 pyramidal cell from CA3 pyramidal cells (S^{Sch}). Separately we analyzed the role of activation of the pre-synaptic CA3 pyramidal cells in driving post-synaptic CA1 pyramidal cells by assigning to each CA1 pyramidal cell a value S^{Pre}, which characterized the average strength of the convergent CA3 inputs to all the CA3 cells that were projecting to a given CA1 cell. Synaptic inhibitory inputs to CA1 pyramidal cells were represented by S^{GABA}, computed by summing the synaptic weights of all GABA connections from CA1 inhibitory neurons to each CA1 pyramidal cell.

Again, we analyzed distribution of the input strength across R-activation scores (Figure 3D). There was a clear trend towards increasing S^{Pre} and S^{Sch} for increasing R-activation of CA1 pyramidal cells, while S^{GABA} and intrinsic excitability did not show any preferential trend for increasing R-activation groups. Only for scores above 75% (very rare in the network, as can be seen in Figure 2F) it appeared that inhibitory synaptic input below the mean could favor high reactivation.

We then used fitting of a multivariate linear model. However, we first separated CA1 pyramidal cells in those with R-activation above and below a threshold of 55% (to satisfy the statistical requirements to perform linear model fitting). As can be seen in Figure 2F, a small portion of all available CA1 pyramidal cells did show R-activation scores above 55%, so it is possible that this sub-group is less representative of the general influence of inputs on R-activation scores, compared to the set of cells

with R-activation scores up to 55%. In studying the large cell pool (below 55%, Table 2) we found a contribution of all inputs (pre-synaptic excitatory input, Schaffer input, inhibitory input and intrinsic excitability), with a tendency for Schaffer input to contribute in relationship to the pre-synaptic excitatory input, rather than independently. When allowing for quadratic terms, the role of direct Schaffer input was rendered null, in favor of heightened influence of pre-synaptic excitatory input and synaptic inhibitory input. When the inputs were considered separately, both excitatory synaptic inputs showed the highest impact on R-activation.

In summary, the interaction of excitatory and inhibitory inputs was significant in modulating CA1 pyramidal cells R-activation, and intrinsic excitability only increased the overall impact of the multivariate model of a minor amount. Mechanistically, this implies that if synaptic activity could change only one of these inputs at a given time, it would have the largest effects on R-activation by modulating either pre-synaptic AMPA connections in CA3, or Schaffer collaterals. We point out that the limited role of intrinsic excitability on R-activation of CA1 pyramidal cells is consistent with our earlier findings on a model of CA1 ripple activity driven by current steps (25).

Table 2. Extract of linear regression models for R-activation of CA1 pyramidal cells (below 55% R-activation) vs inputs (from Table S2)

# Inputs	Inputs in Best Model	Model Equation Type	Adj. R-sq
4	AMPA-Pre,AMPA-Sch,GABA,DC	quadratic, with AMPA-Pre GABA interactions	0.161
3	AMPA-Pre,GABA,DC	quadratic, with AMPA-Pre GABA interactions	0.161
3	AMPA-Pre,AMPA-Sch,DC	Linear + AMPA-Pre AMPA-Sch interaction	0.159
3	AMPA-Pre,AMPA-Sch,GABA	Linear	0.156
2	AMPA-Pre,DC	Linear	0.158
2	AMPA-Pre,GABA	Linear	0.156
1	AMPA-Pre	Quadratic	0.154
1	AMPA-Sch	Linear	0.144
1	GABA	Linear	0.00206
1	DC	Linear	0.00491

For each possible combination of the inputs that were considered (parameters of the model for the statistical linear fit), we found multiple fits to R-activation of CA1 pyramidal cells. When only one input at a time was considered, we found linear models of linear terms and linear models of quadratic terms. When multiple inputs were considered, we found linear models for linear terms, interactions and quadratic terms. The adjusted R^2 terms can be interpreted as a measure of how much of the variance in the data is captured by a given model. As can be seen from the adjusted R^2 values, there was a high noise component in the relationship between inputs and CA1 cells R-activation. However,

the models listed showed significant contributions of the inputs considered (by p-value<0.05 criterion). The complete list of models found is reported in Table S2.

Overall, our analyses revealed: (a) how activation in CA3 and CA1 pyramidal cells during SWRs was controlled by synaptic excitatory inputs in both regions, and (b) the fact that inhibitory synaptic inputs and intrinsic cell excitability only had a significant influence on the R-activation of CA3 pyramidal cells, but not CA1 cells. Differential impact of inhibitory and intrinsic factors in CA1 vs CA3 was likely driven by the fundamentally different activity present in the two separate regions during SWR events. Spiking of CA3 pyramidal cells emerges from reverberating excitatory activity, and could be mediated by post-inhibitory rebound. Spiking in CA1 pyramidal cells is driven by Schaffer Collateral inputs, and local inhibitory signaling competes with such excitatory synaptic input to enforce spike timing of CA1 pyramidal cells during ripple oscillations.

R-activation of cell pairs increases with shared excitatory input

Having established that specific implementation of the network architecture contributed to shaping the R-activation of CA3 and CA1 pyramidal cells, we reasoned that connectivity, and in particular excitatory input, should also contribute to the R-activation of cell pairs. To extend the concept of R-activation score to cell pairs, we considered two cells and their relative order, and found in which percent of the total ripples a given cell pair spiked. Since in our definition of cell pair the order of cell spiking was considered, the R-activation scores of cell pair AB and cell pair BA were in general different. We used our R-activation score measure to group cell pairs with similar reactivation scores in the network, and studied their common synaptic inputs, as described above for single cells (in Figure 3). Below, we analyzed how activation of the cell pairs depended on the network inputs, and we separately tested CA3-CA3, CA1-CA1 and CA3-CA1 pairs.

CA3-CA3 pairs: For pairs of two CA3 pyramidal cells (Figure 4A), we defined an excitatory synaptic input quantifier S^{AMPA}, by finding all pyramidal cells in CA3 which sent synapses to both CA3 cells in the pair and considering the product of the synaptic weights from each of such cells to the cells in the pair (Figure 4A, left panel, shows a drawing of S^{AMPA}). Analogously, the inhibitory input reaching a

pair of CA3 pyramidal cells was quantified by S^{GABA}, summing across all interneurons projecting to both pyramidal cells in the pair the product of the identified synaptic weights (again represented in Figure 4A, left panel). The intrinsic excitabilities of the two cells in the network were considered separately.

Figure 4. Cells that co-reactivate share their input.

A. *Relationship between R-activation scores and input for pairs of CA3 pyramidal cells. Left plot: drawing and formulae introduce the synaptic AMPA and GABA inputs considered (S^{AMPA} and S^{GABA}) for any cell pair labeled (A, B). These estimates quantify the amount of excitatory and inhibitory input that cells A and B have in common. Right plot: R-activation of CA3-CA3 cell pairs is related to strength of synaptic inputs and intrinsic excitability. The bar plot shows on the x –coordinate the average R-activation score of CA3-CA3 cell pairs belonging to the same score group (±5%) and on the y-coordinate the level of each different input (S^{AMPA}, S^{GABA} or Intrinsic Excitability for cell A and for cell B) for cell pairs within that score group. Error bars mark the standard error of the mean. Before grouping cell pairs by their R-activation scores, each input was z-scored to enable comparisons of their respective trends. Therefore, a negative y-coordinate does not reflect a negative input, but an input below the average across the whole network.* ***B.*** *Relationship between cell pair R-activation scores and inputs for pairs of CA1 pyramidal cells. Left plot: drawing and formulae introduce the synaptic inputs considered. For cell pair (A, B) in CA1, excitatory AMPA input from Schaffer collateral alone is labeled S^{Sch}, while the role of the excitability of pre-synaptic cells in CA3 is considered in defining the complementary excitatory synaptic input S^{Pre}. Inhibitory synaptic input S^{GABA} is found analogously to the one for CA3-CA3 cell pairs (in panel* ***A****). These measures are introduced to quantify the shared synaptic inputs between cells A and B in each pair. Right plot: cell pair R-activation scores R-activation of CA1-CA1 cell pairs is related to strength of excitatory synaptic inputs, but not inhibitory synaptic inputs or intrinsic excitability. The bar plot shows on the x –coordinate the average R-activation score of CA1-CA1 cell pairs belonging to the same score group (±5%) and on the y-coordinate the level of each different input (S^{Sch}, S^{Pre}, S^{GABA} or Intrinsic Excitability for cell A and for cell B) for cell pairs within that score group. Error bars mark the standard error of the mean. Before grouping cell pairs by their R-activation scores, each input was z-scored to enable comparisons of their respective trends. Therefore, a negative y-coordinate does not reflect a negative input, but an input below the average across the whole network.* ***C.*** *Relationship between cell pair R-activation scores and inputs for pairs of CA3-CA1 pyramidal cells. Left plot: drawing and formulae introduce the synaptic inputs considered. Excitatory (AMPA-mediated) synaptic inputs are measured as S^{Sch} (which emphasize the role of synaptic paths from cell A in CA3 to cell B in CA1) and S^{Pre} (which emphasizes the role of cells in CA3 connecting to both cell A in CA3 and cell B in CA1). Inhibitory synaptic input is found in CA3 for cell A and in CA1 for cell B, the sum of the two constitutes S^{GABA} for the (A, B) cell pair. These measures are introduced to quantify the shared synaptic inputs between cells A and B in each pair. Right plot: cell pair R-activation scores R-activation of CA3-CA1 cell pairs is related to strength of excitatory synaptic inputs, partly to inhibitory synaptic inputs, but not intrinsic excitability. The bar plot shows on the x –coordinate the average R-activation score of CA3-CA1 cell pairs belonging to the same score group (±5%) and on the y-coordinate the level of each different input (S^{Sch}, S^{Pre}, S^{GABA} or Intrinsic Excitability for cell A and for cell B) for cell pairs within that score group. Error bars mark the standard error of the mean. Before grouping cell pairs by their R-activation scores, each input was z-scored to enable comparisons of their respective trends. Therefore, a negative y-coordinate does not reflect a negative input, but an input below the average across the whole network.*

In Figure 4A, right plot, we show that both excitatory and inhibitory inputs were larger for cell pairs with higher R-activation scores. The intrinsic excitability of the first cell in the network (labeled A in the figure) also increased with R-activation of the pair, while the intrinsic excitability of the second cell in the pair (labeled B in the figure) decreased for higher R-activations. Intuitively, these opposite trends can be understood if one considers that our pair R-activation score is a measure which takes into account the order in which the two cells spiked: intrinsic excitability promotes activation of a cell but in no connection with activity of other cells. Since for a cell pair to repeat in order across ripples it is important that the second cell does not spike de-coupled from the synaptic paths which connect its activity to the first cell, having high intrinsic excitability in the second cell would hinder the R-activation of the pair.

Next, statistical inference analysis of the role played by the different inputs in establishing the R-activation of cell pairs within CA3 was performed with linear regressions (Table 3). It revealed a significant contribution of all inputs and their interactions to the R-activation of cell pairs within CA3. When considering subgroups of inputs, excitatory synaptic input and the intrinsic excitability of the first cell in the pair (and their interaction) could account for a large portion of the modulation of R-activation by all inputs (and interactions). When taken separately, synaptic inputs (both excitatory and inhibitory) still retained an impact on shaping the R-activation of cell pairs, however intrinsic excitability of individual cells had a very small impact on R-activation of CA3-CA3 cell pairs.

Table 3. Extract of linear regression models for R-activation of CA3-CA3 pyramidal cell pairs vs inputs (from Table S3)

# Inputs	Inputs in Best Model	Model Equation Type	Adj. R-sq
4	AMPA-Pre,GABA,DCa,DCb	Quadratic with all interactions	0.258
3	AMPA-Pre,GABA,DCa	Quadratic with all interactions	0.2479
3	AMPA-Pre,DCa,DCb	Quadratic with all interactions	0.244
2	AMPA-Pre,DCa	Quadratic with all interactions	0.234
1	AMPA-Pre	Quadratic	0.165
1	GABA	Quadratic	0.125
1	DCa	Quadratic	0.0658
1	DCb	Linear	0.00392

For each possible combination of the inputs that were considered (parameters of the model for the statistical linear fit), we found multiple fits to R-activation of CA3-CA3 pyramidal cell pairs. When only one input at a time was considered, we found linear models of linear terms and linear models of quadratic terms. When multiple inputs were considered, we found linear models for linear terms, interactions and quadratic terms. The adjusted R^2 terms can be interpreted as a measure of how much of the variance in the data is captured by a given model. As can be seen from the adjusted R^2 values, there was a high noise component in the relationship between inputs and cell pair R-activation. However, the models listed showed significant contributions of the inputs considered (by p-value<0.05 criterion). The complete list of models found is reported in Table S3.

CA1-CA1 pairs: We extended the analysis to pairs of CA1 pyramidal cells, by introducing quantifiers of excitatory and inhibitory inputs (Figure 3). Inhibitory input S^{GABA} was calculated in the same manner as for pairs of CA3 pyramidal cells, meaning we found CA1 inhibitory interneurons projecting to both CA1 pyramidal cells in the pair, multiplied the synaptic strength and summed across all interneurons impinging on both cells in the pair (a representation is shown in Figure 4B, left panel). To quantify the excitatory synaptic inputs reaching a pair of CA1 pyramidal cells, we defined two separate inputs: one considering only the Schaffer Collateral contribution (S^{Sch}) and one emphasizing the role of synaptic paths within CA3 ultimately reaching the cell pair in CA1 (S^{Pre}). The inputs driven by the sole Schaffer Collaterals (S^{Sch}) were quantified by finding cells in CA3 which projected to both cells in the pair (in CA1). The synaptic weights reaching the two cells in the pair were then summed, and these quantities were further summed across all the CA3 pre-synaptic cells found (formula and a drawing are introduced in Figure 4B left panel). The role of CA3 connectivity on the activity of a CA1-CA1 cell pair (S^{Pre}) was quantified by assigning to each cell pair a value, found as follows. We first found paths of two subsequent synapses (di-synaptic paths, from a cell to the next, to the next) starting from one cell in CA3 and terminating on both cells of the CA1 pair (cells in the middle of the di-synaptic paths had to be CA3 pyramidal cells). These initial CA3 cells could drive spiking which impinged (in two synapses) on both cells of the CA1-CA1 cell pair. The synaptic weights along the paths found this way were combined, and further summed across all the possible di-synaptic paths from CA3 to CA1 found in the network (the formula is shown on Figure 4B, left panel). The magnitudes of intrinsic excitability for the two cells in the pair were considered separately.

Figure 4B in the right panel shows how the different input strength changed across R-activation scores. Excitatory synaptic inputs, both in Schaffer Collaterals and within CA3, were higher for cell pairs with higher R-activation scores. In contrast, inhibitory synaptic inputs and intrinsic excitability of either cell in the pair did not show a trend with respect to cell pair R-activation. Hence, we concluded that – consistently with what we found for the R-activation of single CA1 pyramidal cells – only synaptic excitatory inputs could exert an effect on the R-activation of CA1 pyramidal cell pairs.

Statistical inference analysis (Table 4) showed that the synaptic excitatory inputs and their interactions strongly affected R-activation scores of CA1-CA1 pyramidal cell pairs. Inhibitory synaptic input and intrinsic excitability of the cells in the pair did score significantly in the model, but increased minimally the overall ability of the model to represent R-activations. In other words, including inhibitory inputs and intrinsic excitability added great complexity to the model without making significant progress on the representation of R-activations as function of the inputs. Hence, excitatory synaptic inputs greatly dominated all other deterministic inputs in shaping CA1-CA1 cell pair R-activations.

Table 4. Extract of linear regression models for R-activation of CA1-CA1 pyramidal cell pairs vs inputs (from Table S4)

# Inputs	Inputs in Best Model	Model Equation Type	Adj. R-sq
5	AMPA-Pre,AMPA-Sch,GABA,DCa,DCb	Quadratic with all interactions	0.164
4	AMPA-Pre,AMPA-Sch,GABA,DCa	Quadratic with all interactions	0.164
4	AMPA-Pre,AMPA-Sch,GABA,DCb	Quadratic with all interactions	0.163
4	AMPA-Pre,AMPA-Sch,DCa,DCb	Quadratic with all interactions	0.161
3	AMPA-Pre,AMPA-Sch,GABA	Quadratic with all interactions	0.163
3	AMPA-Pre,AMPA-Sch,DCa	Quadratic with all interactions	0.161
3	AMPA-Pre,AMPA-Sch,DCb	Quadratic with all interactions	0.16
2	AMPA-Pre,AMPA-Sch	Quadratic with all interactions	0.16
1	AMPA-Pre	Quadratic	0.106
1	AMPA-Sch	Quadratic	0.149
1	GABA	Quadratic	0.000605
1	DCa	Quadratic	0.00051
1	DCb	Quadratic	$7.81*10^{-5}$

For each possible combination of the inputs that were considered (parameters of the model for the statistical linear fit), we found multiple fits to R-activation of CA1-CA1 pyramidal cell pairs. When only one input at a time was considered, we found linear models of linear terms and linear models of quadratic terms. When multiple inputs were considered, we found linear models for linear terms,

interactions and quadratic terms. The adjusted R^2 terms can be interpreted as a measure of how much of the variance in the data is captured by a given model. As can be seen from the adjusted R^2 values, there was a high noise component in the relationship between inputs and cell pair R-activation. However, the models listed showed significant contributions of the inputs considered (by p-value<0.05 criterion). The complete list of all models found is reported in Table S4.

CA3-CA1 pairs: We finally studied whether the relationship between synaptic input and R-activation would also extend to the cell pairs that spanned the two hippocampal regions composing our network. Since SWR dynamics were organized in a CA3 excitatory event inducing inhibitory oscillations in CA1, we considered only ordered cell pairs in which the first cell was from CA3 and the second from CA1. To define quantifiers for synaptic inputs to pairs of CA3-CA1 pyramidal cells, we again looked for synaptic paths connecting both cells in the pair (showed in Figure 4C, left panel). One direct synaptic input (S^{Pre}), considered CA3 pyramidal cells that projected synapses onto both cells in the pair, and multiplied the two synaptic weights, and summed across all found pre-synaptic cells. Another excitatory synaptic input quantifier (S^{Sch}) was shaped to identify synaptic paths from the first cell in the pair (in CA3) to the second cell in the pair (in CA1), by finding all di-synaptic paths from the first cell in the pair to the second cell in the pair, multiplying the synaptic weights found along the paths and scaling the resulting quantity by the total excitatory synaptic input reaching the first cell in the pair (formula and drawing in Figure 4C). Since each pyramidal cell in the pair could receive inhibition only from interneurons within its same region, the inhibitory synaptic inputs to the two cells in the pair were quantified first separately following the definitions used for single cells in CA3 and in CA1, and the pair inhibitory synaptic input S^{GABA} was computed by the sum of their respective inputs. Intrinsic excitability for each cell in the pair was considered separately.

Once the synaptic and intrinsic deterministic inputs were found, we again plot how the input strength changed across R-activation scores (Figure 4C right panel). We found that excitatory and inhibitory inputs were higher for cell pairs with higher R-activations, while intrinsic excitability of either the first or second cell in the pair had no special trend across R-activation.

To describe the differential role of inputs in shaping the R-activation of CA3-CA1 cell pairs, we derived a statistical inference analysis using multiple variable linear regressions (Table 5). We found a strong dominance of excitatory synaptic inputs over the R-activation scores of CA3-CA1 pairs. When considered separately, pre-synaptic and Schaffer AMPA inputs both accounted for most of the impact of inputs on R-activation, in comparison to the effect found when considering all inputs and all their interactions. In particular, the Schaffer input had the strongest independent impact on R-activations. Furthermore, intrinsic excitability of either cell in the pair, while qualifying for significance in affecting the R-activation score, again did not introduce any strong improvement on the ability of excitatory synaptic inputs (and their interactions) to shape R-activations of CA3-CA1 cell pairs. In summary, what was true for single CA1 pyramidal cells and CA1 cell pairs carries over to CA3-CA1 cells pairs, emphasizing the dominant role of paths of excitatory synaptic connections over inhibitory ones and intrinsic excitability in promoting activation of ordered cell pairs across many SWRs.

Table 5. Extract of linear regression models for R-activation of CA3-CA1 pyramidal cell pairs vs inputs (from Table S5)

# Inputs	Inputs in Best Model	Model Equation Type	Adj. R-sq
5	AMPA-Pre,AMPA-Sch,GABA,DCa,DCb	Quadratic with all interactions (but DCa-DCb)	0.194
4	AMPA-Pre,AMPA-Sch,GABA,DCa	Quadratic with all interactions (but GABA-DCa)	0.193
4	AMPA-Pre,AMPA-Sch,GABA,DCb	Quadratic with all interactions	0.194
4	AMPA-Pre,GABA,DCa,DCb	Quadratic with interactions: AMPA-Pre & GABA, AMPA-Pre & DCa, GABA&DCa, GABA&DCb	0.192
3	AMPA-Pre,AMPA-Sch,GABA	Quadratic with all interactions	0.193
3	AMPA-Pre,GABA,DCa	Quadratic with all interactions	0.191
3	AMPA-Sch,GABA,DCb	Quadratic with all interactions (but AMPA-Sch DCb)	0.192
3	AMPA-Pre,GABA,DCb	Quadratic with all interactions	0.192
2	AMPA-Pre,GABA	Quadratic with all interactions	0.191
1	AMPA-Pre	Linear	0.174
1	DCb	Quadratic	0.00028
1	DCa	Quadratic	8.37*10^-7
1	GABA	Quadratic	0.0106
1	AMPA-Sch	Quadratic	0.168

For each possible combination of the inputs considered (parameters of the model for the statistical linear fit), we found multiple fits to R-activation of CA3-CA1 pyramidal cell pairs. When only one input

at a time was considered, we found linear models of linear terms and linear models of quadratic terms. When multiple inputs were considered, we found linear models for linear terms, interactions and quadratic terms. The adjusted R^2 terms can be interpreted as a measure of how much of the variance in the data is captured by a given model. As can be seen from the adjusted R^2 values, there was a high noise component in the relationship between inputs and cell pair R-activation. However, the models listed showed significant contributions of the inputs considered (by p-value<0.05 criterion). The complete list of all models found is reported in Table S5.

Our analysis across all the possible cell pairs in this network revealed that the spontaneously emergent SWRs in our model encompassed a structured representation of single cells and ordered cell pairs across SWRs, and that such representation was synaptically driven. While the network topology was responsible for the general SWR spiking activity, the specifics of which cells received stronger excitatory synaptic inputs, especially if inputs were considered along synaptic paths which can deliver convergent excitation to a cell pair, exerted selectivity on cells and cell pairs, determining their chances for activation across multiple SWRs in time.

This analysis gives rise to a scenario in which the same network properties which enable the spontaneous emergence of SWRs in the CA3-CA1 architecture (high recurrence in CA3 pyramidal cells, noise-driven spiking in CA3, strong drive to inhibitory neurons in CA1 from CA3 activity) also select a small subset of cells which are most likely to reactivate in a high fraction of SWRs. In other words, our model predicts that replay arises by virtue of the same AMPA/GABA synaptic architecture which generates SWRs themselves. During sleep, the content of hippocampal replay can theoretically be selected within the hippocampal circuitry, and interact with cortical activity by carefully organized timing of SWRs compared to other ongoing oscillations. Within this architecture, memory formation mechanisms during wake (such as STDP, reward signals and awake replay) can modify the chances of specific cells to be replayed during sleep SWRs by altering the relative strengths of synaptic pathways impinging on a group of cells.

Synaptic Plasticity can influence R-activation

Our analysis so far showed a tight relationship between deterministic inputs to cell pairs in the network and their R-activation scores, which suggests that mechanisms capable of modifying such

555 deterministic inputs (such as learning) could in principle modify the R-activation of cell pairs (and
556 hence sequences) in spontaneous SWRs. In the following, we tested whether changing inputs (as
557 defined in the previous section) to a randomly chosen cell pair did in fact result in an increase in its
558 R-activation score.

559 We started by randomly choosing the cell pair, labeled A and B. In a first set of simulations
560 (representing, for example, the sleep on the night before a learning experience, marked with PRE in
561 Figure 5) we found the R-activation score for cell pair AB, together with the deterministic synaptic
562 inputs to AB and intrinsic excitability of A and B. Depending on the type of cell pair considered (CA3-
563 CA3, CA3-CA1 or CA1-CA1) we chose which deterministic inputs were likely to be most impactful on
564 the R-activation score of the cell pair, based on our finding in the previous section. We then re-
565 scaled the strengths of all synaptic connections which contributed to the chosen inputs (and the
566 parameter controlling intrinsic excitability where appropriate), so that in the new connectivity
567 profile the cell pair AB would have larger inputs. We next ran a new simulation, to test how the
568 spontaneous R-activation of the cell pair AB would change for increasing inputs. It is to note that we
569 require that our manipulation preserved the main properties of the spontaneous SWR activity in the
570 network within physiological bounds (i.e. the network did not show constantly firing cells, or highly
571 rhythmically occurring SWRs).

572 ***Figure 5. Increased synaptic strengths promote R-activation of randomly selected cell pairs.***
573 ***A.*** *One example of CA3 cell pair AB randomly chosen in a simulation. Reported on the bar plots are*
574 *its R-activation score, S^{AMPA}, S^{GABA} and the intrinsic excitability of both cell A and B separately. For*
575 *each measured output, the value for the AB pair is shown next to a bar reporting the mean ±standard*
576 *deviation across all pairs of CA3 pyramidal cells (or single cells) in the same simulation. The scaling*
577 *introduced in the network connectivity and intrinsic excitability increased all considered inputs from*
578 *before (PRE, green) to after (POST, red). Note that the mean and standard deviations of the inputs*
579 *across the network do not change from PRE to POST. The R-activation score of AB is near the mean*
580 *in PRE, and larger than one standard deviation above the mean in POST.* ***B.*** *One example of CA3-*
581 *CA1 cell pair AB randomly chosen in a simulation. Reported on the bar plots are its R-activation*
582 *score, S^{Pre}, S^{Sch} and S^{GABA}. For each measured output, the value for the AB pair is shown next to a*
583 *bar reporting the mean ±standard deviation of that value across all pairs of CA3-CA1 pyramidal cells*
584 *in the same simulation. The scaling introduced in the network connectivity increased all considered*
585 *inputs from before (PRE, green) to after (POST, red). Note that the mean and standard deviations of*
586 *the inputs across the network do not change from PRE to POST. The R-activation score of AB is near*
587 *the mean in PRE, and larger than one standard deviation above the mean in POST.* ***C.*** *One example*

of CA1-CA1 cell pair AB randomly chosen in a simulation. Reported on the bar plots are its R-activation score, S^{Pre} and S^{Sch}. For each measured output, the value for the AB pair is shown next to a bar reporting the mean ±standard deviation of that value across all pairs of CA1-CA1 pyramidal cells in the same simulation. The scaling introduced in the network connectivity increased all considered inputs from before (PRE, green) to after (POST, red). Note that the mean and standard deviations of the inputs across the network do not change from PRE to POST. The R-activation score of AB is near the mean in PRE, and larger than one standard deviation above the mean in POST.

Specifically, for pairs of CA3 pyramidal cells, we had previously found (Figure 4A) that excitatory and inhibitory synaptic inputs and intrinsic excitability of the first cell of the pair were larger for higher R-activating cell pairs. Hence, for a randomly chosen pair AB, we scaled synaptic connections contributing to $S^{AMPA}(A,B)$ and $S^{GABA}(A,B)$, and increased the intrinsic excitability of A. The scaling was uniform across all synapses contributing to the inputs, and it was cell pair specific, because its specific value was derived by requiring that the inputs considered will increase at least one standard deviation above the network mean after scaling. As a result, a small percentage of AMPA and GABA synapses within the CA3 network was scaled (less than 0.6% of AMPA and less than 2% of GABA synapses). This led to an increase of the cell pair R-activation score from mean value of approximately 5% to about 20% (more than one standard deviation above the mean, shown in the leftmost bar plot of Figure 5A). In a total of 6 tests of randomly selected cell pairs and simulations, the change of selected inputs and excitability led to increased cell pair R-activation score, while maintaining a network activity profile well within physiological bounds. Hence, for CA3-CA3 pairs, we concluded that uniform scaling of all synapses co-impinging on a pair could promote R-activation of that pair.

For CA3-CA1 cell pairs, we chose to modify both excitatory (S^{Pre} and S^{Sch}) and inhibitory (S^{GABA}) synaptic inputs, since they all showed and increasing trend for increasing R-activation of CA3-CA1 cell pairs (Figure 4C). Hence, our scaling involved AMPA synapses within CA3 and from CA3 to CA1 pyramidal cells, and GABA synapses within CA3 and within CA1. In one example of a randomly selected CA3-CA1 cell pair AB, shown in Figure 5B, the synaptic manipulation resulted in increased excitatory and inhibitory synaptic inputs on cell pair AB, while the mean and standard deviation of each input was not altered (the change affected less than 2% of AMPA synapses within CA3, less

than 0.5% of Schaffer collaterals, less than 3% of GABA synapses in CA3 and about 12% of GABA synapses in CA1). The change in synapses produced a significant increase of AB R-activation score, from ~7% to more than 30%. Among a total of 6 randomly selected CA3-CA1 cell pairs and simulations, analogous manipulations resulted in increased R-activation score for the cell pair in 4 cases, while all tests showed SWR activity within physiological bounds.

Finally, to study the effect of synaptic scaling on the R-activation of a CA1-CA1 cell pair, we elected to modify only the excitatory synaptic inputs reaching the cell pair (S^{Pre} and S^{Sch}, defined in Figure 4B), since inhibitory synaptic inputs and intrinsic excitability of either cell in the pair did not show a clear increasing trend for increasing R-activation score across CA1-CA1 cell pairs (Figure 4B). In one example of randomly selected AB CA1-CA1 cell pair (Figure 5C), both excitatory synaptic inputs increased due to our synaptic scaling procedure, and AB R-activation score grew from about 2% to above 15%. In contrast to other types of cell pairs, we found that for CA1-CA1 cell pairs the scaling of excitatory synaptic inputs very often affected the network dynamics. In a total of 11 randomly selected cell pairs and simulations which resulted in increased AB R-activation, most of them (9 samples) showed an exaggerated amount of SWRs in network activity following synaptic scaling. This was likely due to the much larger fraction of excitatory synapses being modified by the scaling procedure (about 5% of all AMPA synapses between CA3 pyramidal cells, and 0.05% of Schaffer collaterals) compared to other types of cell pairs. To avoid this pitfall, we studied the complementary problem: whether reducing the input to a randomly selected CA1-CA1 cell pair would cause a reduction in the cell pair R-activation score. In a total of 7 randomly selected cell pairs and simulations, we scaled synapses within CA3 pyramidal cells and from CA3 pyramidal cells to CA1 pyramidal cells to reduce the S^{Pre} and S^{Sch} on pair AB. As expected, in all tests the network activity remained physiological, and we found in 5 tests that the synaptic manipulation resulted in lower R-activation score for the selected cell pair.

We conclude that this artificial manipulation was effective at increasing R-activation in cell pairs as long as it did not affect a large fraction of excitatory cells (hence sending the network activity out of balance). We predict that physiological synaptic plasticity aimed to increase excitatory synaptic inputs to a CA1-CA1 cell pair which is part of a memory trace will not influence all synaptic paths leading to the pair but rather modify synapses within a specific subset of CA3 and CA1 cells (a cell assembly). The choice of which cells and synapses will be affected by learning-driven plasticity would likely depend on the specific spiking of cells during behavior. In other words, our study suggests that the reactivation of a cell assembly during ripples in CA1 really derives from the generalized reactivation of a CA3-CA1 cell assembly, which – according to our results – is established by plastic modulation of excitatory synaptic paths within CA3 and Schaffer collaterals, inhibitory synaptic paths within both CA3 and CA1, and the intrinsic excitability of CA3 pyramidal cells.

Discussion

In this paper, we introduced a spiking network of CA3-CA1 activity showing spontaneously emergent, localized, stochastic SWRs. Within these events, we studied the spike reactivation in CA3 and CA1 during SWRs, and measured the fraction of ripples in which a cell spiked with a "ripple-activation" (R-activation) score between 0 and 100%. When compared to a stationary sampling process, we found that a relatively rigid network architecture (defined by stationary probability distributions of intrinsic and synaptic cell properties) shaped the spiking of low R-activating cells (the majority), while network dynamics (dependent on the specific implementation of the network configuration) shaped the activity of highly R-activating cells. We further found that the degree to which a cell activated across ripples was modulated by the amount of synaptic excitatory and inhibitory input received by the cell. In particular, for CA3 cells but not for CA1 cells, we found a role for intrinsic cell excitability in shaping cell activation across ripples. This observation generalized to cell pairs and synaptic paths which impinge on both cells composing the pair, meaning that a shared pathway of synaptic input could promote co-activation of cell pairs. Furthermore, we showed that

666 increasing the shared synaptic input of a cell pair could lead to increased R-activation. Together,
667 these observations are indicative of a network-wide coordination of activation probability across
668 SWRs for cells and cell pairs, which is further refined by specific synaptic strengths. This suggests a
669 possible competition for R-activation among cell assemblies, where synaptic strengths mediate the
670 chance of dominance of a given memory over others during spontaneous SWRs.

671 ## Model captures both generic ripple activity and potential mechanisms of learning-dependent
672 replay

673 CA1 place cells recruited during encoding of recent experience are known to reactivate together
674 during subsequent sleep (14). Importantly, rather than displaying a uniform probability of spiking
675 during ripples, cells can be divided in those which are active during SWRs and those which are not, a
676 feature that persists across recordings (3, 24). The precise manner in which *in vivo* SWRs involve or
677 exclude a specific pyramidal cell from their activity remains unknown. Our model predicts that
678 synaptic plasticity during learning (such as, e.g., mediated by awake SWR activity (31, 37, 38)) could
679 effectively cause the inclusion of cells coding for a novel learned task in the set of CA1 pyramidal
680 cells which are spiking during sleep SWRs (24). Hence, we propose that SWRs frame activation of a
681 generic representation within which spikes from the specific place cells involved in recently encoded
682 experience are preferentially engaged, gated by recent synaptic plasticity.

683 ## Other models of SWR and hippocampal replay

684 The biophysical model of CA3-CA1 SWR activity which we propose in this study builds on a vast
685 literature on the mechanisms of ripples and sharp waves. *In vitro* and *in vivo* studies have shown
686 that in CA1 ripples are dominated by inhibitory phasic activity (39, 40), and basket cells spike at high
687 frequency (39, 41) in localized groups (26). Meanwhile, pyramidal cells spike relatively rarely, phase-
688 locked to windows of opportunity left by the ongoing oscillatory inhibitory signal (22, 33). In CA3,
689 excitatory and inhibitory spiking is not locked to CA1 ripple waves (30), and can emerge
690 spontaneously (39, 42) *in vitro*, while *in vivo* its initiation is still under investigation (23, 43). In the

691 search for explanatory mechanisms underlying SWRs, numerous possible strategies have been
692 introduced. Gap junctions between CA3 pyramidal cells have been proposed to be necessary (44, 45)
693 but experimental evidence is still not definitive for such mechanism (3, 46, 47). Models which take
694 advantage of supra-linear summation of post-synaptic potentials among CA3 and CA1 pyramidal
695 cells have proposed that SWRs are synaptically propagating waves, where each excitatory spike
696 induces its own local feedback inhibitory activity (48, 49). These assume a very similar activity in CA3
697 and CA1 during SWRs, and depend strictly on the presence of strong excitatory synapses between
698 CA1 cells (which have been found to be very few (50)). In work by Taxidis et al. (51), AMPA and GABA
699 receptor-mediated synaptic activity, combined with intrinsic bursting of CA3 pyramidal cells, are the
700 basic mechanisms underlying the emergence of SWRs in a computational model which can be seen
701 as a precursor to our model. In the model by Taxidis, SWRs have to happen rhythmically, because
702 their initiation is crucially tied to the bursting activity in the CA3 recurrent network: that model
703 requires that CA3 pyramidal cells spike in bursts, and do so in strong synchrony in every theta cycle.
704 In our model, SWRs occur stochastically, with long stochastic pauses in between packets of events,
705 consistent with *in vivo* findings (52). This physiologically realistic result arises from taking into
706 consideration the crucial role played by background noisy activity in setting the SWR mechanism.

707 In previous work (25), we introduced a model of CA1 receiving direct current (a simplified sharp
708 wave). In that model, ripples in CA1 were represented by transient orbits of a dynamical system in
709 which ripple activity is initiated by a synchronizing input to interneurons, then activity winds around
710 a fixed point inducing fast decaying oscillations, and termination is due to heterogeneity among the
711 interneurons driving the transient orbit back to the stationary (de-synchronized) state. Here, we
712 introduce sharp wave activity in CA3 which is an escape process. The CA3 network has strong
713 recurrence of excitatory synapses, and CA3 pyramidal cells are in a noise-driven spiking regime,
714 which means that spikes are driven by fluctuations in the incoming currents (including synaptic
715 ones). This imposes a disorganized state in the network (LIA, found during slow wave sleep in the
716 hippocampus (3)), and SWRs emerging when enough CA3 pyramidal cells spike in a small window of

717 time. This leads part of the network to organize, accumulating recruitment of other pyramidal cells
718 and interneuron spikes until the network cannot sustain its propagation any further. This implies
719 that sparseness in the CA3 recursive synapse architecture is also a necessary property of our model
720 design.

721 Our model design for sharp wave activity is similar to the one introduced by Omura et al. (36), which
722 particularly addressed the lognormal distribution of firing rates found across CA3 activity and its
723 relationship to a specific distribution in the synaptic weights of excitatory connections in the
724 network. In their model, hippocampal activity is isolated from external input, apart from a short-
725 lived initial Poisson drive. Our new model is a complete CA3-CA1 spontaneous activity design, where
726 sharp waves and ripples are built to be different phenomena, one mainly excitatory, marked by
727 wave propagation and extending to a large portion of the excitatory population, one mainly
728 inhibitory, rhythmic and involving a small fraction of local pyramidal cells. In our model, cells receive
729 colored noise to represent the ongoing activity of all other inputs (for example from entorhinal
730 cortex) present *in vivo* (53). Furthermore, we focus on how this structure is capable of supporting
731 replay mediated by AMPA and GABA synapses, which is not addressed in Omura et al. The ability of
732 selective connections to promote cell assembly reactivation (spontaneous and evoked) has been
733 analyzed recently by (54) who show that synaptic strengths among cells in one assembly can
734 promote burst-reactivation, considering both excitatory and inhibitory cells as part of the assembly.
735 In our study, we consider spikes of pyramidal cells to represent information content and spikes of
736 inhibitory cells to contribute to the shape of overall network dynamics (ending a sharp wave in CA3,
737 and pacing the frequency of ripples in CA1). This idea is consistent with experimental data which has
738 found a heightened specificity in the activation of hippocampal pyramidal cells compared to
739 hippocampal interneurons across the various rhythmic activities which mark different phases in
740 information processing in an *in vivo* task (55).

Summary and predictions for reactivation

We believe our model is the first which addresses the mechanisms of localized activity not only in CA1 (ripples), but also in CA3 (sharp waves). Our study further expands the possibilities on how hippocampal reactivation during sleep can interact with ongoing activity in cortex and other brain structures. It predicts that topologically organized input (from CA2 or directly from mossy fibers) could selectively activate a given portion of CA3 and foster reactivation which is specific to that area (a local SWR event). The spiking content which is then reactivated (the precise spike sequence) in CA3-CA1 will depend on the specific to synaptic connections within CA3 and between CA3 and CA1. Such replay could then be passed downstream (through subiculum and its targets) back to cortex and other structures, in an ongoing loop aimed at changing synapses outside the hippocampus based on the content of hippocampal replay activated through selective projections from upper layers of entorhinal cortex to dentate gyrus (and hence CA3). For this overall consolidation to take place, and hence perform a share-and-transfer of information from hippocampus to cortex during slow wave sleep, ripples need to be flexible in their timing, while their content needs to be stable, but able to be evoked differentially depending on the overall input activity (replay is known to change due to auditory stimulation during sleep (32), for example). Furthermore, for consolidation to take place, SWRs need to be able to reactivate recent and past events to foster the integration of new factual events in generalized conceptual schemas which enable the animal (and humans) to use its experiences to comprehend the world surrounding it (hence, generalize). A CA3-CA1 network which is too rigid, too rhythmic, or too dependent on few supra-linear connections in its specific SWR activity, will find it harder to support flexible spiking to mediate consolidation across a night of sleep.

Materials and Methods

Network Model: rationale

We started with our previously developed (25) network of CA1 pyramidal and basket cells and constructed a network of pyramidal and basket cells to represent CA3 activity, then built Schaffer Collaterals projecting CA3 pyramidal cells to CA1 pyramidal cells and interneurons. We used equations of the adaptive exponential integrate and fire formalism (56, 57), which can show bursting activity (like CA3 and CA1 pyramidal cells (58)) or fast-spiking activity (like basket cells (58)) depending on their parameters (57). CA3 pyramidal cells were allowed a stronger tendency to burst in response to a current step input by having a less strong spike frequency adaptation than CA1 neurons (58). For simplicity, all cells belonging to the same population had the same parameters (specified in the following section). To introduce heterogeneity among cells in the network, every cell received a different direct current term (selected from a normal distribution)), and every cell received an independent Ornstein–Uhlenbeck process (OU process) (59), which can be thought of as a single-pole filtered white noise, with cutoff at 100Hz. This noisy input was added to take into account the background activity of the cells which we did not explicitly model in the network. The standard deviation of the OU process controlled the size of the standard deviation in sub-threshold fluctuations of cell voltages, and was a parameter kept fixed within any cell type. Once the parameter tuning was in effect, the cells (even when disconnected from the network) were showing fast and noisy sub-threshold voltage activity, and their spikes were non-rhythmic, driven by fluctuations in the noise input they received, which is called a noise-driven spiking regime, rather than a deterministic spiking regime, and is representative of *in vivo* conditions (60-62).

Cells were arranged within a one-dimensional network in CA3 (see Figure 1A), and connectivity within CA3 was characterized by each cell reaching other cells within a third of the network around them (Figure 1B), which is consistent with anatomical estimates (28). For pyramidal to pyramidal cells connections, the probability of synaptic contact within this radius of one third was higher for

788 neurons closer to the pre-synaptic cell and decayed for neurons further away. Details of all network
789 connections are introduced in the Network Model: connectivity section. Intuitively, the highly
790 recurrent connections between pyramidal cells in CA3 had a gradient in density that resulted in a
791 convergence/divergence connectivity fairly uniform across all CA3 pyramidal cells, which represents
792 the overall homogeneity of CA3 pyramidal cells arborization within the region Overall, this
793 connectivity represents the highly recurrent pyramidal connections in CA3 without introducing
794 special hubs of increased excitatory recurrence in any specific location in the network.

795 ## Network Model: equations and parameters

796 We model SWR activity in the hippocampus using a network of 240 basket cells and 1200 pyramidal
797 cells in CA3, 160 basket cells and 800 pyramidal cells in CA1. The ratio of excitatory to inhibitory
798 neurons is known to be approximately 4 (58) and since in our model we did not introduce any of the
799 numerous hippocampal interneuron types but for basket cells, we apply that ratio to the pyramidal
800 to basket cell network. This ratio also favored the ability of the network to support a background
801 disorganized spiking regime, where excitatory and inhibitory currents were able to balance each
802 other (53). For each neuron, the equations are

$$C\,\dot{v} = -g_L(v - E_L) + g_L\Delta\, exp\left(\frac{(v - V_t)}{\Delta}\right) - w + I(t)$$

$$\tau_w \dot{w} = a(v - E_L) - w$$

$$v(t) = V_{thr} \Rightarrow v(t + dt) = V_r, w(t + dt) = w(t) + b$$

$$I(t) = I_{DC} + \beta\eta_t + I_{syn}(t)$$

$$\tau\, d\eta_t = -\eta_t\, dt + dW_t$$

$$I_{inp}(t) = I_{max}\left(1 + \exp\left(-\frac{t - t_{on}}{k}\right)\right)^{-1}\left(1 + \exp\left(\frac{t - t_{off}}{k}\right)\right)^{-1}$$

803 CA1 cells parameters are reported in (25), and CA3 cells parameters were as follows. Pyramidal cells
804 parameters: C (pF) = 200; g_L (nS) = 10; E_L (mV)= -58; A = 2; b (pA) = 40; Δ (mV) = 2; τ_w (ms) = 120; V_t

(mV) = -50; V_r (mV) = -46; V_{thr} (mV) = 0. Interneurons parameters: C (pF) = 200; g_L (nS) = 10; E_L (mV)= -70; A = 2; b (pA) = 10; Δ (mV) = 2; τ_w (ms) = 30; V_t (mV) = -50; V_r (mV) = -58; V_{thr} (mV) = 0.

The coefficients establishing noise size were β = 80 for pyramidal cells, β = 90 for interneurons. DC inputs were selected from Gaussian distributions with mean 24 (pA) and standard deviation 30% of the mean for pyramidal cells in CA3, mean 130 (pA) and standard deviation 30% of the mean for CA3 interneurons, mean 40 (pA) and standard deviation 10% of the mean for CA1 pyramidal cells and mean 180 (pA) and standard deviation 10% of the mean for CA1 interneurons.

Synaptic currents were modeled with double exponential functions, for every cell n we had $Isyn\,(t) = \sum_{j=1}^{160} g^{j\to n}\, s^{j\to n}(t)(v_n - E_i) + \sum_{j=1}^{800} g^{j\to n}\, s^{j\to n}(t)(v_n - E_e)$,

where $E_i = -80$ mV and $E_e = 0$ mV, and $s^{j\to n}(t) = \sum_{t_k} F\left(e^{H\left(\frac{t-t_k}{\tau_D}\right)} - e^{H\left(\frac{t-t_k}{\tau_R}\right)}\right)$, where t_k are all the spikes of pre-synaptic cell *j*.

In this equation, F is a normalization coefficient, set so that every spike in the double exponential within parentheses peaks at one, and $H(\cdot)$ is the Heaviside function, ensuring that the effect of each pre-synaptic spike affects the post-synaptic current only after the spike has happened. The time scales of rise and decay (in ms) used in the model were as follows (25, 51, 63, 64). For AMPA connections from pyramidal cells to pyramidal cells: τ_R = 0.5, τ_D = 3.5. For AMPA connections from pyramidal cells to interneurons: τ_R = 0.5, τ_D = 3. For $GABA_A$ connections from interneurons to interneurons: τ_R = 0.3, τ_D = 2. For $GABA_A$ connections from interneurons to pyramidal cells: τ_R = 0.3, τ_D = 3.5.

Network Model: connectivity

The CA3 network was organized as a one-dimensional network. For connections from a CA3 pyramidal cell to the other CA3 pyramidal cells, we first considered a radius (of about one third of the network) around the presynaptic cell, and the probability of connection from the presynaptic cell

828 to any cell within such radius was higher for cells with indeces nearby the presynaptic cell and
829 reduced progressively with cell index distance (28). Specifically, we used a cosine function to shape
830 the probability within the radius, and parameterized how fast with index distance the probability
831 had to decay by using a monotonic scaling of the cosine phase: if x was the index distance within the
832 network, y = arctan(kx)/arctan(k) imposed the decay probability p(y) = Pcos(4y), where P was the
833 peak probability and k= 2 was a parameter controlling the decay of connection probability with
834 distance within the radius. An analogous structure underlid the probability of CA3 pyramidal cells to
835 connect to inhibitory interneuron in CA3 and for Schaffer Collaterals to connect a CA3 pyramidal cell
836 to CA1 pyramidal cells (28). To balance the relationship between feed-forward excitation from
837 pyramidal cells to interneurons and feedback inhibition from interneurons to pyramidal cells,
838 probability of connection from a presynaptic basket cell to a cell within a radius (about 1/3 of the
839 network size) was constant at 0.7, for $GABA_A$ connections to both CA3 pyramidal cells and
840 interneurons. Within CA1 connectivity was all-to-all, with the caveat that synaptic weights which
841 were sampled at or below zero caused a removal of a given synapse. As a result, most synapses
842 between CA1 pyramidal cells were absent, consistently with experimental findings (50). To introduce
843 heterogeneity among synaptic connections, synaptic weights for all synapse types were sampled
844 from Gaussian distributions with variance (σ) given by a percent of the mean (μ). Parameters used in
845 the simulations were (we use the notation Py3 and Py1 to denote pyramidal cells in CA3 and CA1,
846 respectively and analogously Int3/Int1 for interneurons). Py3->Py3: μ = 34, σ = 40%μ; Int3->Int3: μ =
847 54, σ = 40%μ; Py3->Int3: μ = 77, σ = 40%μ; Int3->Py3: μ = 55, σ = 40%μ; Py3->Py1: μ = 34, σ = 10%μ;
848 Py3->Int1: μ = 320, σ = 10%μ; Int1->Int1: μ = 3.75, σ = 1%μ; Py1->Int1: μ = 6.7, σ = 1%μ; Int1->Py1: μ
849 = 8.3, σ = 1%μ; Py1->Py1: μ = 0.67, σ = 1%μ. It is to note that the mean (μ) declared was normalized
850 by the total number of cells before the variance to the mean was introduced in the distribution.
851 Since the CA3 and CA1 networks are of different sizes, a direct comparison of the parameter values
852 or their magnitude across regions would not account for the effective values used in the simulations.

853

854 ## Acknowledgments:

855 PM and MB work supported by ONR grant (MURI: N000141612829 and N000141612415) to MB, MJ

856 work supported by A Wellcome Trust Senior Research Fellowship in Basic Biomedical Science

857 202810/Z/16/Z. The authors thank Dr. Giri Krishnan for helpful discussions.

858

References

1. Krishnan GP, Chauvette S, Shamie IS, Soltani S, Timofeev I, Cash SS, et al. Cellular and Neurochemical Basis of Sleep Stages in Thalamocortical network. eLife. 2016;Under Review.

2. Lee SH, Dan Y. Neuromodulation of brain states. Neuron. 2012;76(1):209-22.

3. Buzsaki G. Hippocampal sharp wave-ripple: A cognitive biomarker for episodic memory and planning. Hippocampus. 2015;25(10):1073–188.

4. Buzsaki G, Leung LW, Vanderwolf CH. Cellular bases of hippocampal EEG in the behaving rat. Brain Res. 1983;287(2):139-71.

5. Mizuseki K, Royer S, Diba K, Buzsáki G. Activity Dynamics and Behavioral Correlates of CA3 and CA1 Hippocampal Pyramidal Neurons. Hippocampus. 2012;22(8):1659-80.

6. Sirota A, Buzsaki G. Interaction between neocortical and hippocampal networks via slow oscillations. Thalamus Relat Syst. 2005;3(4):245-59.

7. Molle M, Born J. Slow oscillations orchestrating fast oscillations and memory consolidation. Progress in brain research. 2011;193:93-110.

8. Eschenko O, Ramadan W, Molle M, Born J, Sara SJ. Sustained increase in hippocampal sharp-wave ripple activity during slow-wave sleep after learning. Learning & memory (Cold Spring Harbor, NY). 2008;15(4):222-8.

9. Ramadan W, Eschenko O, Sara SJ. Hippocampal sharp wave/ripples during sleep for consolidation of associative memory. PloS one. 2009;4(8):e6697.

10. Girardeau G, Benchenane K, Wiener SI, Buzsaki G, Zugaro MB. Selective suppression of hippocampal ripples impairs spatial memory. Nat Neurosci. 2009;12(10):1222-3.

11. Ego-Stengel V, Wilson MA. Disruption of ripple-associated hippocampal activity during rest impairs spatial learning in the rat. Hippocampus. 2010;20(1):1-10.

12. Marshall L, Helgadottir H, Molle M, Born J. Boosting slow oscillations during sleep potentiates memory. Nature. 2006;444(7119):610-3.

885 13. Ji D, Wilson MA. Coordinated memory replay in the visual cortex and hippocampus during
886 sleep. Nat Neurosci. 2007;10(1):100-7.
887 14. Wilson MA, McNaughton BL. Reactivation of hippocampal ensemble memories during sleep.
888 Science. 1994;265(5172):676-9.
889 15. Skaggs WE, McNaughton BL. Replay of neuronal firing sequences in rat hippocampus during
890 sleep following spatial experience. Science. 1996;271(5257):1870-3.
891 16. Sutherland GR, McNaughton B. Memory trace reactivation in hippocampal and neocortical
892 neuronal ensembles. Curr Opin Neurobiol. 2000;10(2):180-6.
893 17. Hoffman KL, McNaughton BL. Coordinated reactivation of distributed memory traces in
894 primate neocortex. Science. 2002;297(5589):2070-3.
895 18. Schwindel CD, McNaughton BL. Hippocampal-cortical interactions and the dynamics of
896 memory trace reactivation. Progress in brain research. 2011;193:163-77.
897 19. Foster DJ, Wilson MA. Reverse replay of behavioural sequences in hippocampal place cells
898 during the awake state. Nature. 2006;440(7084):680-3.
899 20. Wu X, Foster DJ. Hippocampal replay captures the unique topological structure of a novel
900 environment. The Journal of neuroscience : the official journal of the Society for Neuroscience.
901 2014;34(19):6459-69.
902 21. Diekelmann S, Born J. The memory function of sleep. Nat Rev Neurosci. 2010;11(2):114-26.
903 22. Csicsvari J, Hirase H, Czurko A, Mamiya A, Buzsaki G. Fast network oscillations in the
904 hippocampal CA1 region of the behaving rat. The Journal of neuroscience : the official journal of the
905 Society for Neuroscience. 1999;19(16):Rc20.
906 23. Csicsvari J, Hirase H, Mamiya A, Buzsáki G. Ensemble patterns of hippocampal CA3-CA1
907 neurons during sharp wave-associated population events. Neuron. 2000;28(2):585-94.
908 24. Grosmark AD, Buzsaki G. Diversity in neural firing dynamics supports both rigid and learned
909 hippocampal sequences. Science. 2016;351(6280):1440-3.

910 25. Malerba P, Krishnan GP, Fellous JM, Bazhenov M. Hippocampal CA1 Ripples as Inhibitory
911 Transients. PLoS computational biology. 2016;12(4):e1004880.
912 26. Patel J, Schomburg EW, Berenyi A, Fujisawa S, Buzsaki G. Local generation and propagation
913 of ripples along the septotemporal axis of the hippocampus. The Journal of neuroscience : the
914 official journal of the Society for Neuroscience. 2013;33(43):17029-41.
915 27. Shepherd GM. The synaptic organization of the brain. 5th ed. Oxford ; New York: Oxford
916 University Press; 2004. xiv, 719 p.
917 28. Li XG, Somogyi P, Ylinen A, Buzsáki G. The hippocampal CA3 network: an in vivo intracellular
918 labeling study. J Comp Neurol. 1994;339(2):181-208.
919 29. Ylinen A, Bragin A, Nadasdy Z, Jando G, Szabo I, Sik A, et al. Sharp wave-associated high-
920 frequency oscillation (200 Hz) in the intact hippocampus: network and intracellular mechanisms. The
921 Journal of neuroscience : the official journal of the Society for Neuroscience. 1995;15(1 Pt 1):30-46.
922 30. Sullivan D, Csicsvari J, Mizuseki K, Montgomery S, Diba K, Buzsáki G. Relationships between
923 hippocampal sharp waves, ripples, and fast gamma oscillation: influence of dentate and entorhinal
924 cortical activity. The Journal of neuroscience : the official journal of the Society for Neuroscience.
925 2011;31(23):8605-16.
926 31. Atherton LA, Dupret D, Mellor JR. Memory trace replay: the shaping of memory
927 consolidation by neuromodulation. Trends in neurosciences. 2015;38(9):560-70.
928 32. Carr MF, Karlsson MP, Frank LM. Transient slow gamma synchrony underlies hippocampal
929 memory replay. Neuron. 2012;75(4):700-13.
930 33. Csicsvari J, Hirase H, Czurko A, Mamiya A, Buzsaki G. Oscillatory coupling of hippocampal
931 pyramidal cells and interneurons in the behaving Rat. The Journal of neuroscience : the official
932 journal of the Society for Neuroscience. 1999;19(1):274-87.
933 34. Anastassiou CA, Montgomery SM, Barahona M, Buzsaki G, Koch C. The effect of spatially
934 inhomogeneous extracellular electric fields on neurons. The Journal of neuroscience : the official
935 journal of the Society for Neuroscience. 2010;30(5):1925-36.

936 35. Mizuseki K, Buzsaki G. Preconfigured, skewed distribution of firing rates in the hippocampus
937 and entorhinal cortex. Cell reports. 2013;4(5):1010-21.
938 36. Omura Y, Carvalho MM, Inokuchi K, Fukai T. A Lognormal Recurrent Network Model for
939 Burst Generation during Hippocampal Sharp Waves. The Journal of neuroscience : the official journal
940 of the Society for Neuroscience. 2015;35(43):14585-601.
941 37. O'Neill J, Senior T, Csicsvari J. Place-selective firing of CA1 pyramidal cells during sharp
942 wave/ripple network patterns in exploratory behavior. Neuron. 2006;49(1):143-55.
943 38. Girardeau G, Zugaro M. Hippocampal ripples and memory consolidation. Curr Opin
944 Neurobiol. 2011;21(3):452-9.
945 39. Schlingloff D, Káli S, Freund TF, Hájos N, Gulyás AI. Mechanisms of Sharp Wave Initiation and
946 Ripple Generation. The Journal of neuroscience : the official journal of the Society for Neuroscience.
947 2014;34(34):11385-98.
948 40. Gan J, Weng SM, Pernia-Andrade AJ, Csicsvari J, Jonas P. Phase-Locked Inhibition, but Not
949 Excitation, Underlies Hippocampal Ripple Oscillations in Awake Mice In Vivo. Neuron.
950 2017;93(2):308-14.
951 41. Varga C, Golshani P, Soltesz I. Frequency-invariant temporal ordering of interneuronal
952 discharges during hippocampal oscillations in awake mice. Proc Natl Acad Sci U S A.
953 2012;109(40):E2726-34.
954 42. Maier N, Nimmrich V, Draguhn A. Cellular and network mechanisms underlying spontaneous
955 sharp wave-ripple complexes in mouse hippocampal slices. J Physiol. 2003;550(Pt 3):873-87.
956 43. Oliva A, Fernandez-Ruiz A, Buzsaki G, Berenyi A. Role of Hippocampal CA2 Region in
957 Triggering Sharp-Wave Ripples. Neuron. 2016;91(6):1342-55.
958 44. Traub RD, Wong RK, Miles R, Michelson H. A model of a CA3 hippocampal pyramidal neuron
959 incorporating voltage-clamp data on intrinsic conductances. J Neurophysiol. 1991;66(2):635-50.

960 45. Traub RD, Bibbig A. A model of high-frequency ripples in the hippocampus based on synaptic
961 coupling plus axon-axon gap junctions between pyramidal neurons. The Journal of neuroscience :
962 the official journal of the Society for Neuroscience. 2000;20(6):2086-93.
963 46. Buhl DL, Harris KD, Hormuzdi SG, Monyer H, Buzsaki G. Selective impairment of hippocampal
964 gamma oscillations in connexin-36 knock-out mouse in vivo. The Journal of neuroscience : the official
965 journal of the Society for Neuroscience. 2003;23(3):1013-8.
966 47. Stark E, Roux L, Eichler R, Senzai Y, Royer S, Buzsáki G. Pyramidal cell-interneuron
967 interactions underlie hippocampal ripple oscillations. Neuron. 2014;83(2):467-80.
968 48. Jahnke S, Timme M, Memmesheimer RM. A Unified Dynamic Model for Learning, Replay,
969 and Sharp-Wave/Ripples. The Journal of neuroscience : the official journal of the Society for
970 Neuroscience. 2015;35(49):16236-58.
971 49. Memmesheimer RM. Quantitative prediction of intermittent high-frequency oscillations in
972 neural networks with supralinear dendritic interactions. Proc Natl Acad Sci U S A.
973 2010;107(24):11092-7.
974 50. Deuchars J, Thomson AM. CA1 pyramid-pyramid connections in rat hippocampus in vitro:
975 dual intracellular recordings with biocytin filling. Neuroscience. 1996;74(4):1009-18.
976 51. Taxidis J, Coombes S, Mason R, Owen MR. Modeling sharp wave-ripple complexes through a
977 CA3-CA1 network model with chemical synapses. Hippocampus. 2012;22(5):995-1017.
978 52. Davidson TJ, Kloosterman F, Wilson MA. Hippocampal Replay of Extended Experience.
979 Neuron. 2009;63(4):497-507.
980 53. Atallah BV, Scanziani M. Instantaneous modulation of gamma oscillation frequency by
981 balancing excitation with inhibition. Neuron. 2009;62(4):566-77.
982 54. Chenkov N, Sprekeler H, Kempter R. Memory replay in balanced recurrent networks. PLoS
983 computational biology. 2017;13(1):e1005359.
984 55. Rangel LM, Rueckemann JW, Riviere PD, Keefe KR, Porter BS, Heimbuch IS, et al. Rhythmic
985 coordination of hippocampal neurons during associative memory processing. Elife. 2016;5:e09849.

986 56. Touboul J, Brette R. Dynamics and bifurcations of the adaptive exponential integrate-and-
987 fire model. Biological cybernetics. 2008;99(4-5):319-34.
988 57. Brette R, Gerstner W. Adaptive Exponential Integrate-and-Fire Model as an Effective
989 Description of Neuronal Activity. Journal of Neurophysiology. 2005;94(5):3637-42.
990 58. Andersen P, Morris R, Amaral D, Bliss T, O'Keefe J. The hippocampus book: Oxford University
991 Press; 2006.
992 59. Uhlenbeck GE, University of Michigan AAaPLdRUU, Holland, Ornstein LS, University of
993 Michigan AAaPLdRUU, Holland. On the Theory of the Brownian Motion. Physical Review.
994 1930;36(5):823.
995 60. Broicher T, Malerba P, Dorval AD, Borisyuk A, Fernandez FR, White JA. Spike phase locking in
996 CA1 pyramidal neurons depends on background conductance and firing rate. The Journal of
997 neuroscience : the official journal of the Society for Neuroscience. 2012;32(41):14374-88.
998 61. Fernandez FR, Broicher T, Truong A, White JA. Membrane voltage fluctuations reduce spike
999 frequency adaptation and preserve output gain in CA1 pyramidal neurons in a high-conductance
1000 state. The Journal of neuroscience : the official journal of the Society for Neuroscience.
1001 2011;31(10):3880-93.
1002 62. Roxin A, Brunel N, Hansel D, Mongillo G, van Vreeswijk C. On the distribution of firing rates
1003 in networks of cortical neurons. The Journal of neuroscience : the official journal of the Society for
1004 Neuroscience. 2011;31(45):16217-26.
1005 63. Bartos M, Vida I, Frotscher M, Meyer A, Monyer H, Geiger JR, et al. Fast synaptic inhibition
1006 promotes synchronized gamma oscillations in hippocampal interneuron networks. Proc Natl Acad Sci
1007 U S A. 2002;99(20):13222-7.
1008 64. Cutsuridis V, Graham B, Cobb S, Vida I. Hippocampal microcircuits: a computational
1009 modeler's resource book: Springer Science & Business Media; 2010.

1010

1011 # Figures

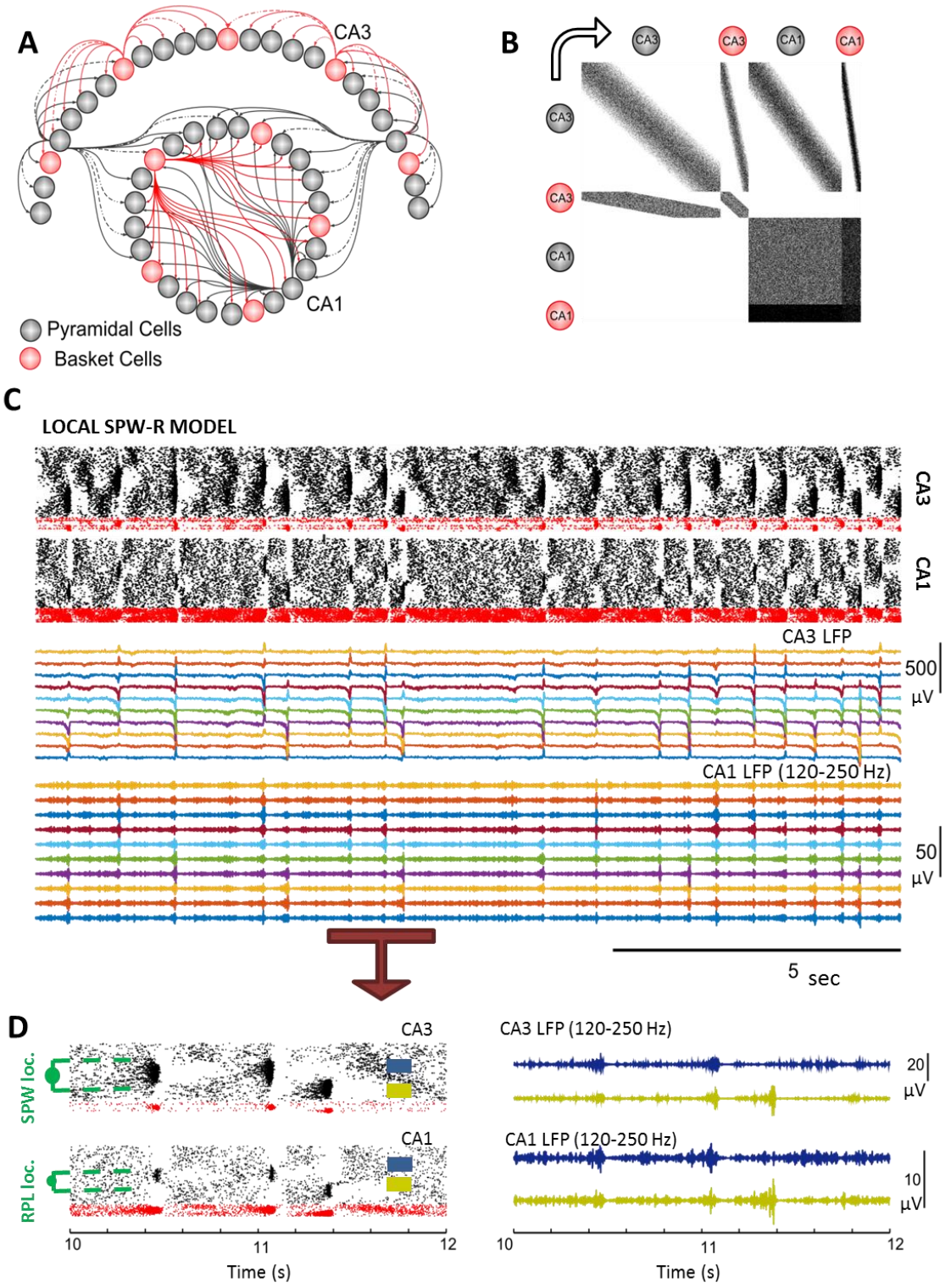

1012
1013 **FIGURE 1**

1014

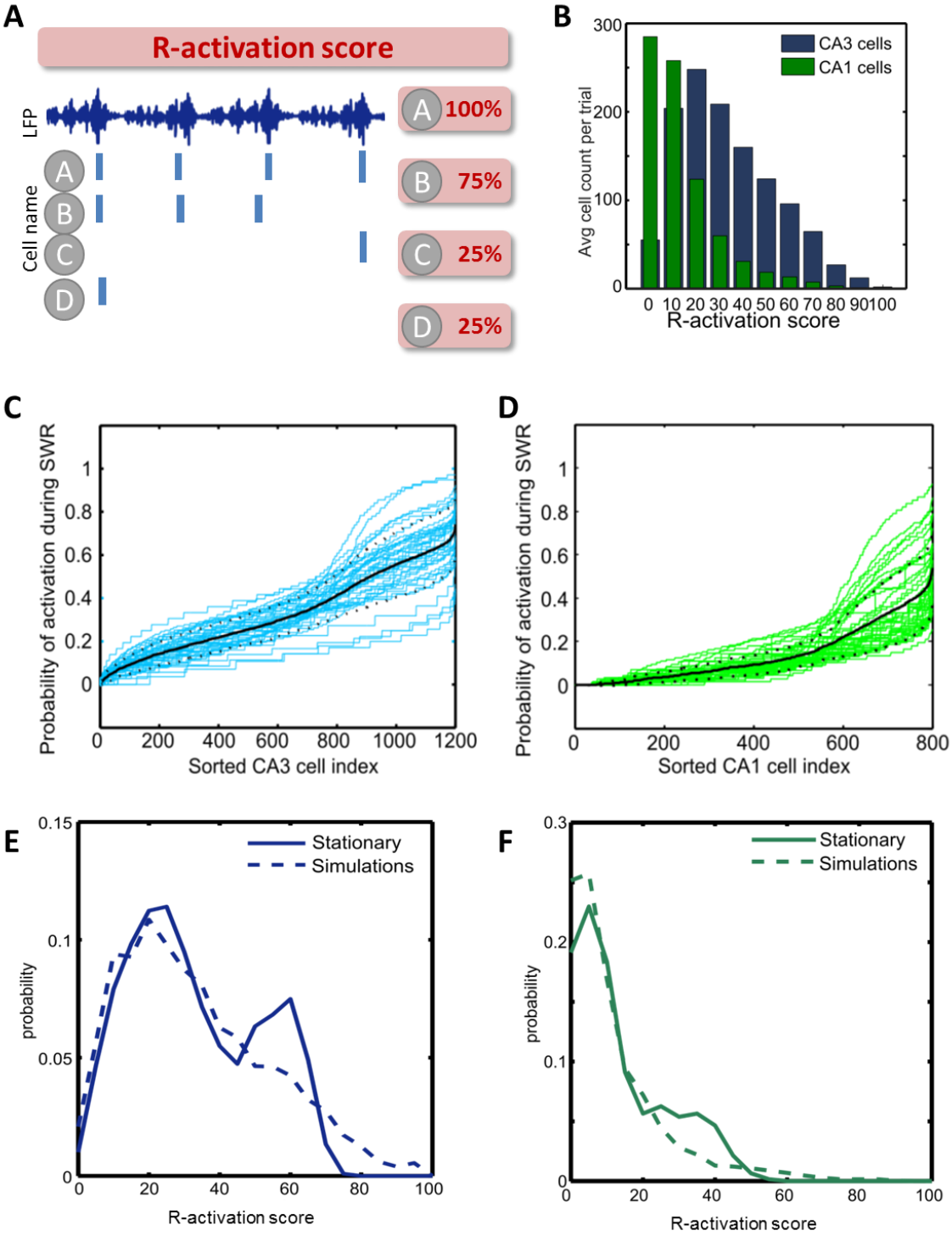

1015

1016 **FIGURE 2**

1017

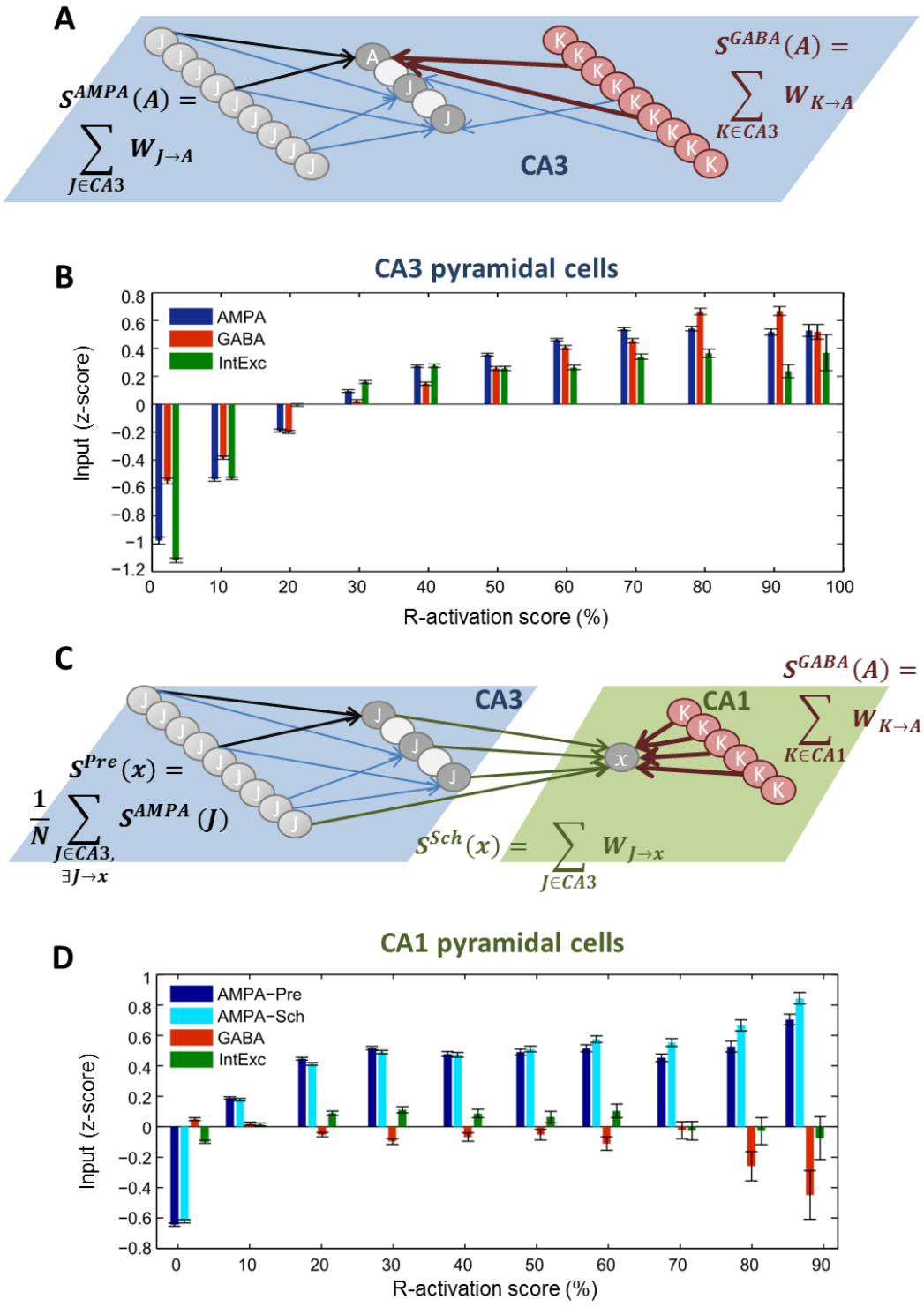

FIGURE 3

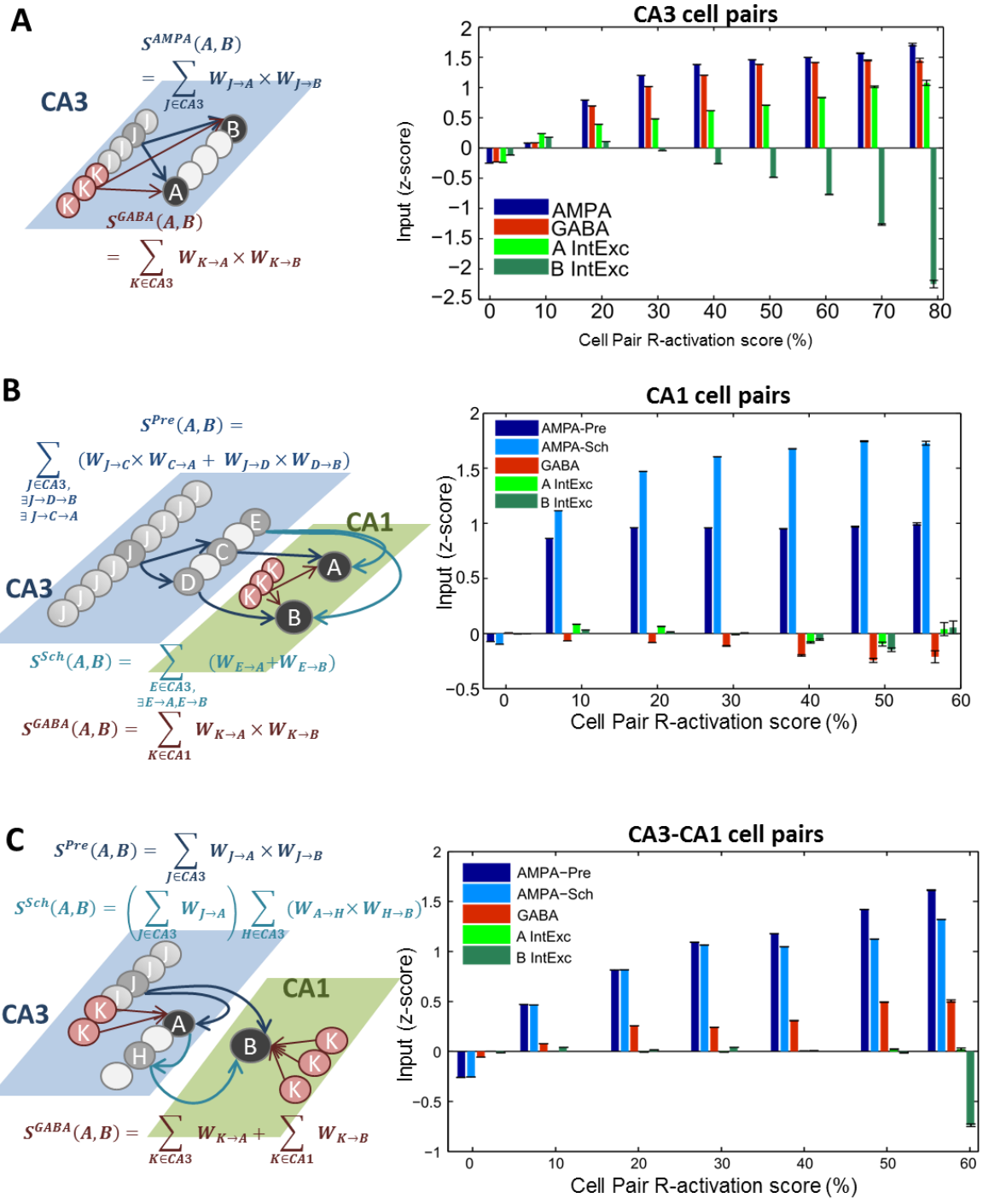

FIGURE 4

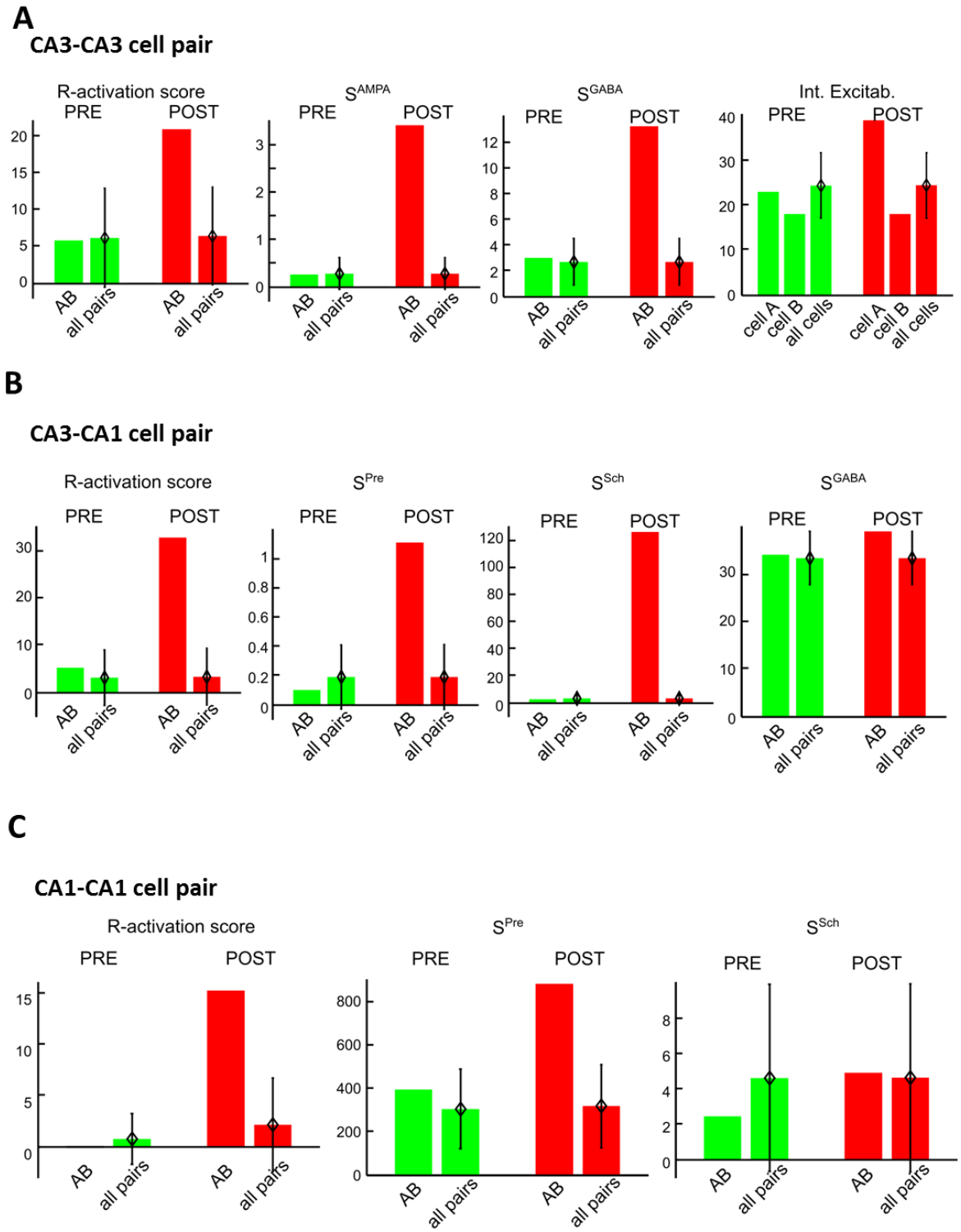

1024

1025 **FIGURE 5**